INL/EXT-22-68181

Advanced Measurement and Visualization Techniques for High-Temperature Heat Pipe Experiments

July 2022

Sunming Qin, Luis Nunez III, Zachary Sellers, Jeremy Hartvigsen, Piyush Sabharwall, Scott Thompson
Idaho National Laboratory

Robert Reid
Los Alamos National Laboratory

Victor Petrov
University of Michigan – Ann Arbor

Joseph Seo, Yassin Hassan
Texas A&M University

Philippe Bardet
The George Washington University

MRP Microreactor Program

INL Idaho National Laboratory

INL is a U.S. Department of Energy National Laboratory operated by Battelle Energy Alliance, LLC

INL/EXT-22-68181

Advanced Measurement and Visualization Techniques for High-Temperature Heat Pipe Experiments

Sunming Qin, Luis Nunez III, Zackary Sellers, Jeremy Hartvigsen, Piyush Sabharwall, Scott Thompson
Idaho National Laboratory

Robert Reid
Los Alamos National Laboratory

Victor Petrov
University of Michigan – Ann Arbor

Joseph Seo, Yassin Hassan
Texas A&M University

Philippe Bardet
The George Washington University

July 2022

Idaho National Laboratory
Nuclear Science & Technology
Idaho Falls, ID, USA 83415

http://www.inl.gov

Prepared for the
U.S. Department of Energy
Office of Nuclear Energy
Under DOE Idaho Operations Office
Contract DE-AC07-05ID14517

Page intentionally left blank

SUMMARY

This report conducts a preliminary investigation of the available literature and summarizes some potential advanced measurement and visualization techniques for operating high-temperature heat pipe (HP) that can be implemented to support the United States (U.S.) Department of Energy (DOE) Microreactor Program (MRP). The primary objective for the extensive literature research is to investigate the possibilities and feasibility for the design and construction of an advanced experimental test facility with the aim of producing high-fidelity high-resolution heat pipe data during its operation.

Based on the existing HP test facilities at Idaho National Laboratory (INL)—including the Single Primary Heat Extraction and Removal Emulator (SPHERE) and the Microreactor Agile Non-Nuclear Experimental Test Bed (MAGNET)—further efforts will be made to examine the technical feasibility to HP measurements and support the research, development, and demonstration (RD&D) process for an HP-cooled microreactor. Continuing collaborations with the Nuclear Energy Advanced Modeling and Simulation (NEAMS) program, other research institutes and universities are considered to be extremely important so that the experimental facility and resultant database can satisfy the validation needs of advanced heat pipe modeling codes being developed under DOE NEAMS program.

Page intentionally left blank

ACKNOWLEDGMENTS

This research was supported by the U.S. Department of Energy–Office of Nuclear Energy (DOE–NE) MRP under DOE Contract No. DE-AC07-05ID14517. The authors also recognize and appreciate the feedback and support given by Dr. Victor Petrov's research group from the University of Michigan, Prof. Hassan's group from Texas A&M University and Prof. Philippe Bardet from the George Washington University.

Page intentionally left blank

CONTENTS

FIGURES

TABLE

Page intentionally left blank

ACRONYMS

Al	Aluminum
AM	Advanced Manufacturing
Ar	Argon
atm	Atmosphere
Cu	Copper
DC	Direct Current
DIC	Digital Image Correlation
DLP	Digital Light Photoluminescence
DOE	U.S. Department of Energy
DOE–NE	U.S. Department of Energy–Office of Nuclear Energy
DTS	Distributed Temperature Sensor
g	Gram
GWU	George Washington University
He	Helium
HP	Heat Pipe
HTGR	High-Temperature Gas-cooled Reactor
HX	Heat Exchanger
INL	Idaho National Laboratory
IR	Infrared
kW	Kilowatt
LMHP	Liquid Metal Heat Pipe
LTHPF	Low-Temperature Heat Pipe Test Facility
m	Meter
MAGNET	Microreactor Agile Non-Nuclear Experimental Test Bed
MOOSE	Multiphysics Object-Oriented Simulation Environment
MRP	Microreactor Program
MWe	Megawatt Electrical
MWth	Megawatt Thermal
NEAMS	Nuclear Energy Advanced Modeling and Simulation
Na	Sodium
Ni	Nickel
NRC	U.S. Nuclear Regulatory Commission

ORNL	Oak Ridge National Laboratory
PCU	Power Conversion Unit
RD&D	Research, Development, and Demonstration
SCR	Silicon-Control-Rectifier
SPHERE	Single Primary Heat Extraction and Removal Emulator
TAMU	Texas A&M University
TDLAS	Tunable Diode Laser Absorption Spectroscopy
UAM	Ultrasonic Additive Manufacturing
UM	University of Michigan
U.S.	United States
V&V	Verification and Validation
W	Watt

Advanced Measurement and Visualization Techniques for High-Temperature Heat Pipe Experiments

1. INTRODUCTION AND BACKGROUND

Microreactor systems produce a stable, continuous supply of abundant energy in a relatively small footprint. For microreactors, specific deployment opportunities may include the provision of heat and electrical power to remote commercial and industrial applications, remote civilian municipalities, or remote or isolated military installations. Typical power needs in these types of facilities range from 1 to 10 megawatts electrical (MWe) power. In many current applications, power generation at this scale is achieved through the use of diesel generators. However, increasing costs, clean-energy goals, and supply-chain constraints have prompted a desire to examine other options to ensure energy availability and reliability. Microreactors generally produce about 0.1 to 50MWe[a]. They are factory manufacturable, easily transportable, and, due to neutronic simplicity, allow for semi- or fully autonomous operation. To ensure accelerated deployment the United States (U.S.) Department of Energy (DOE) Microreactor Program (MRP) [1] is working closely with vendors, the U.S. Nuclear Regulatory Commission (NRC), and other DOE programs to develop capabilities to enable successful demonstration. Various types of microreactor designs are under consideration; among those, the heat pipe (HP)-cooled reactor designs, as illustrated in Figure 1, are currently being actively investigated at Idaho National Laboratory (INL). To support non-nuclear testing and demonstration of technology under the MRP, the Single Primary Heat Extraction and Removal Emulator (SPHERE) and Microreactor Agile Non-Nuclear Experimental Test Bed (MAGNET) were designed and constructed to perform high-temperature HP experiments at INL. The novel and unique experimental database will be of great value and importance to support the computational code development and guide the advanced microreactor system design.

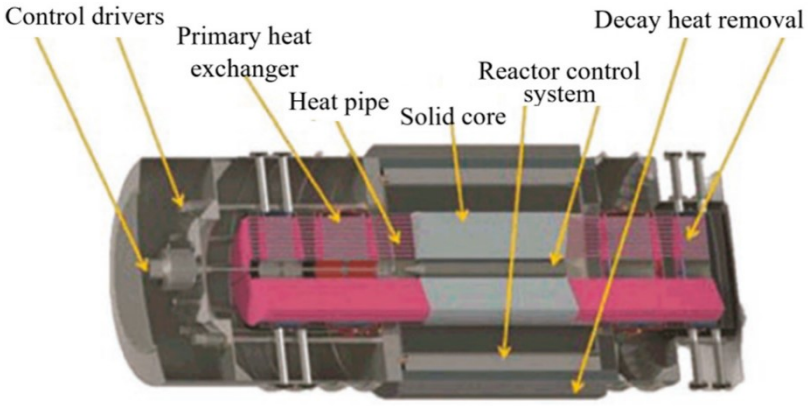

Figure 1. Heat-pipe-cooled microreactor design concept. Adapted from [2].

Some information, such as the permanent mechanical deformations caused by plastic strain or thermal creep, can be gleaned from post-test examination of microreactor components subjected to electrical heating and temperature gradients that are representative of expected conditions during nuclear operation. However, the major benefits to performing electrically heated experiments—besides not having to work with nuclear fuel, reactor constraints, and activated materials—are the ability to incorporate more detailed instrumentation during the tests and better control of the environmental conditions. Non-nuclear experiments, which will be performed with SPHERE and MAGNET, will provide detailed distributions of the thermomechanical parameters (i.e., temperature and strain) and quantify the fundamental

[a] Infrastructure and Jobs Act of 2021

limitations of microreactor components and systems, including heat-rejection capabilities of HPs and advanced HXs.

Meanwhile, software verification and validation (V&V) hold an important role in the safety analysis for nuclear facilities, as the codes and models utilized in calculations demonstrating the safety basis as part of DOE authorization must demonstrate an acceptable pedigree. The DOE Nuclear Energy Advanced Modeling and Simulation (NEAMS) program is developing tools for HP applications, currently under development, is called Sockeye [3], and is based on the Multiphysics Object-Oriented Simulation Environment (MOOSE) [4] finite element framework. Recently, the MRP technical report [5] pointed out the need to address V&V gap that exists for Sockeye development, and need for more comprehensive experimental data—preferably the internal measurements during HP operation which is crucial for accurate modeling. Therefore, to construct high-quality high-fidelity database, advanced measurement techniques are being considered to better understand HP internal physics.

2. HEAT PIPE: PHYSICS AND MEASUREMENT

In the past several decades, HPs are becoming increasingly popular, and are being recognized as one of the most efficient passive heat transfer technologies that is available. Therefore, HPs have been employed in a wide variety of thermal applications—including micro-electronics cooling, vehicle thermal management, and energy storage/recovery systems [6-8]. Of the various types of available HPs, our particular interest lies in the liquid metal heat pipes (LMHPs), which use alkali metals as a working fluid. Given that LMHPs can offer a reliable and effective way of thermal management for high-temperature thermal systems, great attention has been paid from various industries to build solar collectors [8], advanced nuclear reactors [9, 10], space power systems [11-13], etc.

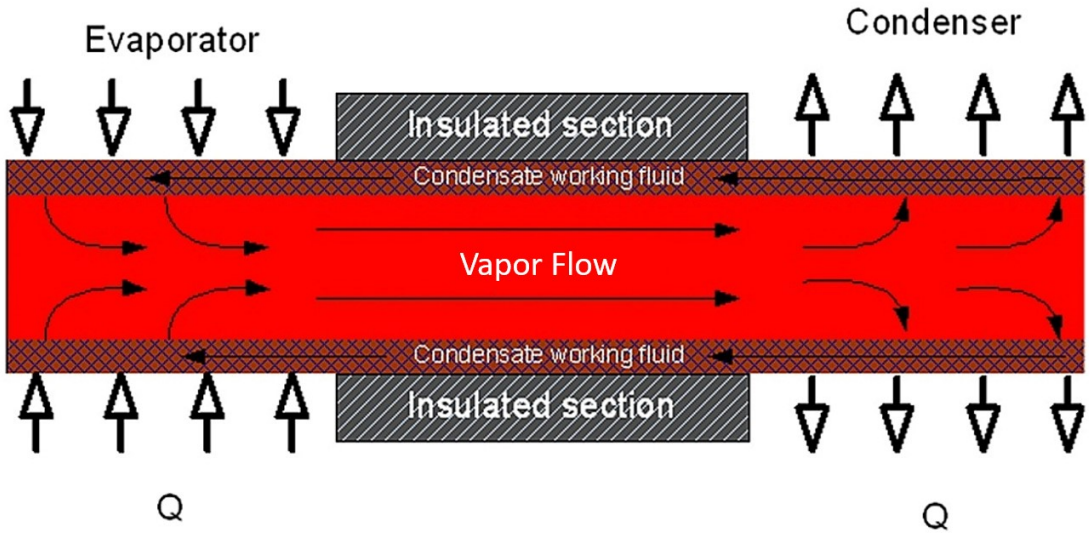

Figure 2. The HP working cycle. Adapted from [14].

In general, HPs are passive thermal transfer devices with the ability to transport large amounts of heat over relatively long distances, with no moving parts, but instead using phase change processes and vapor diffusion. The main structure of a HP consists of an evacuated tube partially filled with a working fluid that exists in both liquid and vapor phases. Figure 2 represents the basic steps of HP operation, which is a continuous cycle. When the HP is heating up, the working fluid is allowed to evaporate. The difference in densities between the vapor and the fluid, as well as the resultant pressure gradient between the evaporator and condenser parts, allows the vapor to reach the cool condenser section. The difference in wall temperature causes the vapor to condensate and release the latent heat, thereby allowing the fluid to

return to the liquid pool located in the evaporator by capillary forces in the wicking structures [15]. To better understand the physics and measurement challenges of the LMHPs, this section provides a brief overview of the HP operating limits and proposes some parameters of interest for high-temperature LMHP experiments.

2.1 Heat Pipe Operating Limits

As mentioned for the HP-cooled microreactor designs investigated by the MRP, the HP design consists of stainless-steel encasements filled with a liquid metal working fluid—typically either potassium or sodium. While HPs are straightforward and reliable devices, they are subject to several heat transport limitations that must be considered for safe operation. These limits are plotted in Figure 3, and can be described as follows [16]:

1. ***Capillary Limit*:** This limit is encountered when the liquid in the evaporator is evaporated at a greater rate than it can be returned to the evaporator due to insufficient capillary-driving pressure as compared to the pressure losses around the circuit.
2. ***Entrainment Limit:*** This limit occurs when the vapor phase is able to shear off liquid from the wick surface into the central channel, thus limiting the flow of liquid to the evaporator.
3. ***Boiling Limit:*** This limit occurs when nucleate boiling occurs in the evaporator at such a rate that bubble formation and departure inhibit the return of liquid to the evaporator.
4. ***Viscous Limit:*** This limit occurs when the vapor pressure is insufficient to overcome the pressure drop along the pipe, thus shortening its distance into the condenser region.
5. ***Sonic Limit:*** This limit occurs when the vapor flow is choked at the evaporator exit.

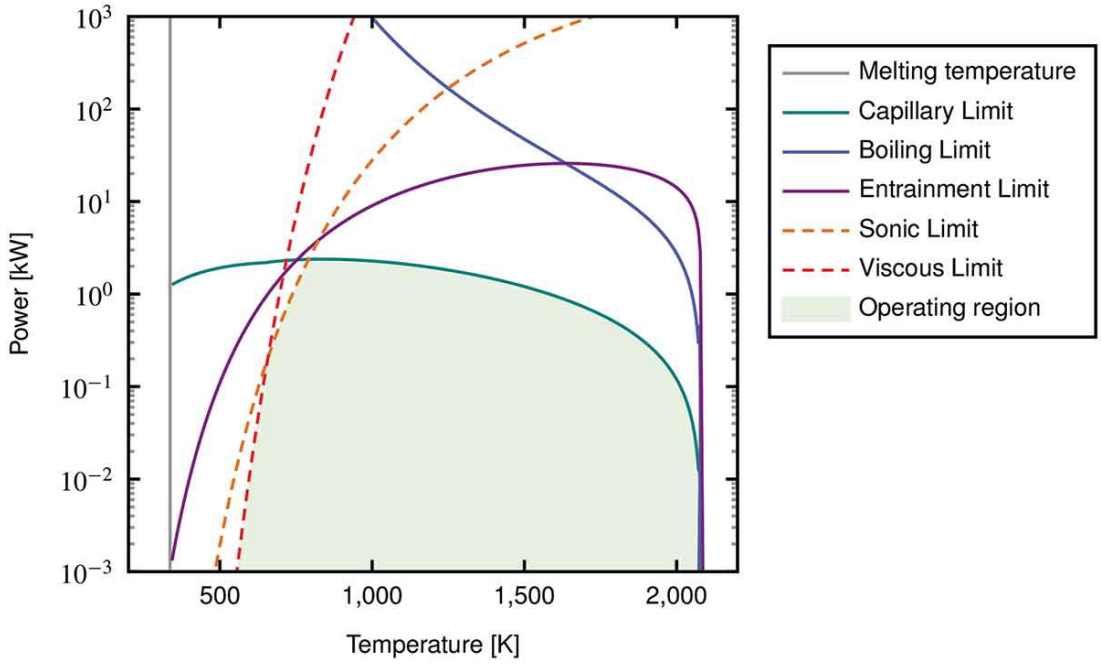

Figure 3. Analytical HP operation limits calculated by Sockeye. The two bounding limits that do not result in catastrophic failure of the HP are the sonic and viscous limits, that are represented with dashed lines which effectively limit the amount of heat flux that can be transferred by the HP. Adapted from [16].

Matthews et al. [16] pointed out that of these five limits, the capillary, boiling, and entrainment limits are considered ‘catastrophic’ HP failures from which normal operation is not recoverable without a

reactor shutdown. The remaining two limits are considered 'bounding' limits, resulting in decreased heat fluxes at the evaporator and condenser side of the HP. If the temperature were to change to more favorable conditions away from the bounding limits, the heat flux would then return to normal operation, as designated by the shaded region in Figure 3. Although HPs retain a limited ability to transfer heat to the secondary side via conduction through the HP casing, the rate of heat transfer through the steel HP casing is significantly smaller than the heat flux realized by operating HPs, so this heat transfer mechanism is typically ignored. In addition to the five operational limits described previously, the extremely low temperatures of HPs are limited by the freezing point of the working fluid, which becomes essential during cold startup or shutdown. Lastly, failures due to casing breaches, which result in the loss of the working fluid, can also result in 'catastrophic' failure of the HP.

In general, HPs provide a high-level of confidence in robustness and reliability due to the lack of moving parts and sealed design. Although the primary risk to a microreactor is the loss of heat removal, most modern core design will likely be able to handle failure of one or two HPs. Consequently, cascade failure is often considered a primary failure mode that needs to be avoided and will be investigated and analyzed in near future in MAGNET testbed to support the MRP.

2.2 Measurement Variables of Interest

As recognized and acknowledged by the code development community, the V&V process of any numerical methods and physical models in advanced modeling and simulation are part of best practices. These steps are necessary so that vendors employing the software for design and safety applications have confidence in the validity of computational results. The key to developing a useful advanced modeling and simulation capability for a given physical system is a rigorous validation paradigm primarily founded in integrating advanced modeling and simulation development with a stringent multiscale, multiphysics experimental program that is repeatable and delivers data with quantifiable uncertainties [16].

According to the Sockeye development manual [17], as well as the computational modeling needs to support the microreactor development and demonstration program [18, 19], advanced measurement techniques are needed to obtain the following properties with high accuracy and repeatability:

- Temperature on internal and external side of the HP during the full operation cycle
- Stress and displacement measurement for the containment holding the HP
- Internal measurement of void fraction and film thickness for operating HPs
- Vapor velocity in the HP core during operation
- Sodium vapor pressure inside the HPs at different operating stages.

These quantities are extremely arduous to measure due to the high operating temperature of LMHPs. In addition, the stainless-steel sheath of the HP makes it impossible to visualize the internal part with traditional optic measurement techniques. Based on these measurement needs—as well as the challenges—an extensive literature review will be presented with the available and possible advanced manufacturing capabilities in section 3.3, and advanced measurement techniques in section 3.3, respectively.

3. EXPERIMENTAL FACILITIES AND CAPABILITITES

The primary experimental hardware capabilities currently under development are focused on non-nuclear thermal and integrated systems testing and the development of test articles to perform experiments—specifically, this includes SPHERE and MAGNET. The capabilities described in this section will generate data that will further support other DOE programs and industrial needs. These data will be made available to researchers and developers for a range of testing purposes to support model development and V&V efforts.

3.1 SPHERE Facility

The SPHERE facility is equipped with a test chamber that allows for either vacuum (10^{-4} torr) or inert gas operation. The SPHERE facility process flow diagram is shown in Figure 4. Cooling water is recirculated using a 2.5 kilowatt (kW) circulating chiller unit. The water flow loop includes a precision turbine flow meter and a delta-T meter that will allow for accurate determination of the heat removal rate from the HP to the cooling water. Prior to testing, the quartz tube is evacuated using a vacuum pump and then backfilled with inert gas consisting either of helium (He) or argon (Ar). This process is repeated several times by successive dilution at the beginning of each test to ensure that all the air has been removed. An oxygen sensor provides a second validation of total removal of air from the system. Measurement of HP axial temperature profiles during startup, steady-state, and transient operations involve using thermal imaging and surface-temperature measurement, performing calorimetric measurements with a water-cooled gas-gap calorimeter, determining HP operational limits, and testing under both vacuum and inert gas conditions [20]. The objectives of the single HP testing include:

1. Documentation of HP thermal performance under a wide range of heating values and operating temperatures
2. Observation of HP startup and transient operation
3. Development of effective thermal-coupling methods between the outer surface of the HP and the core block and between the cartridge heaters and the core block.

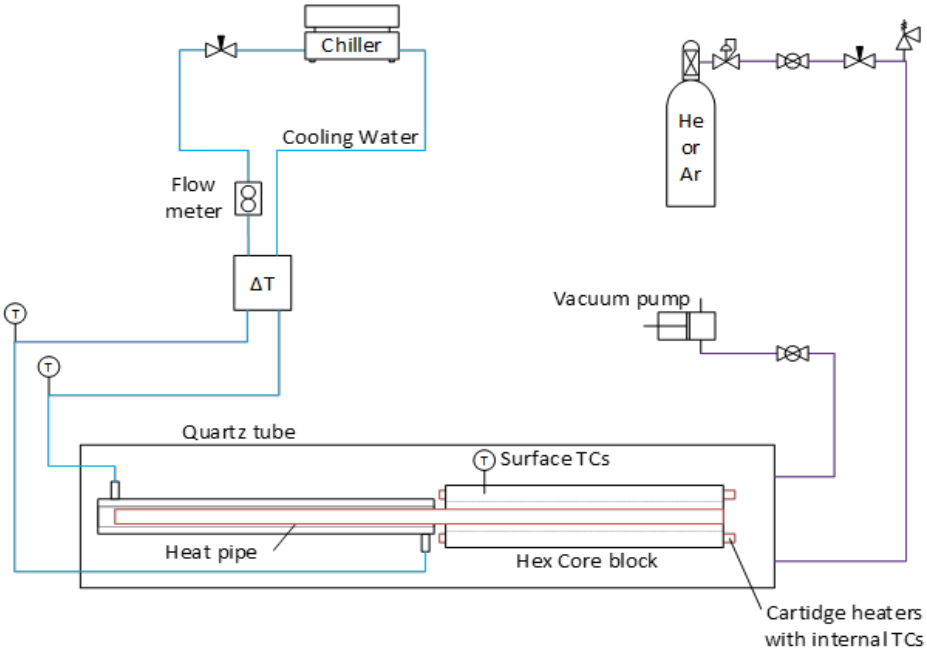

Figure 4. Piping and instrumentation diagram for the SPHERE facility.

Thermal performance of the operating HPs will be determined by measurement of HP heat removal capacity as a function of operating temperature. The heat removal rate is equal to the total heater power input, measured by power meters, minus any heat losses as determined by a combination of direct measurement by calorimetry measurements and an analysis of temperature gradients through the block and along the HP. The body of these HPs is stainless-steel. The working fluid is sodium, and the wick structure is specific to the supplier. The total quantity of sodium in each HP is small, roughly 60–80 grams (g). After charging, the HPs are welded shut. From the standpoint of our operations, the HPs are fully closed, fully sealed test articles. The design basis surface heat flux value for the cartridge heaters is 3.8 W/cm^2, based on expected microreactor core power densities. For the 6 in. block, this power density yields 317 watt (W) per heater and a total power of 1891 W. For the 1/2-meter (m) block with the same power densities, each heater would operate at 1 kW, for a total power of 6 kW. For the 1-m block, each heater would operate at 2 kW, for a total power of 12 kW. During testing in SPHERE, the heat fluxes that can be applied will be limited by the heat transfer rating of the HPs. This limitation will result in the use of significantly lower heat fluxes than the full prototypical core design values, especially for the longer core blocks. Heater operating temperatures will be limited to 750°C. Note that the vapor pressure of sodium is still well below 1 atmosphere (atm) at this temperature. Therefore, over-pressurization failure of the HP is not a concern.

The single HP experiments will be performed using a 7-hole hexagonal core block with the cross-sectional geometry shown in Figure 5(a). The core block material is stainless-steel 316L. Three different core block lengths have been fabricated: 0.152-m, 0.5-m, and 1-m. A photograph of one of the hex blocks is presented in Figure 5(b). The outer ring of six holes in the core block will be fitted with cartridge heaters designed to mimic heating from microreactor fuel rods and the center hole will be occupied by the HP. The gaps between the HP, heaters, and hex block are filled with boron nitride paste to ensure a perfect thermal contact during the experiments.

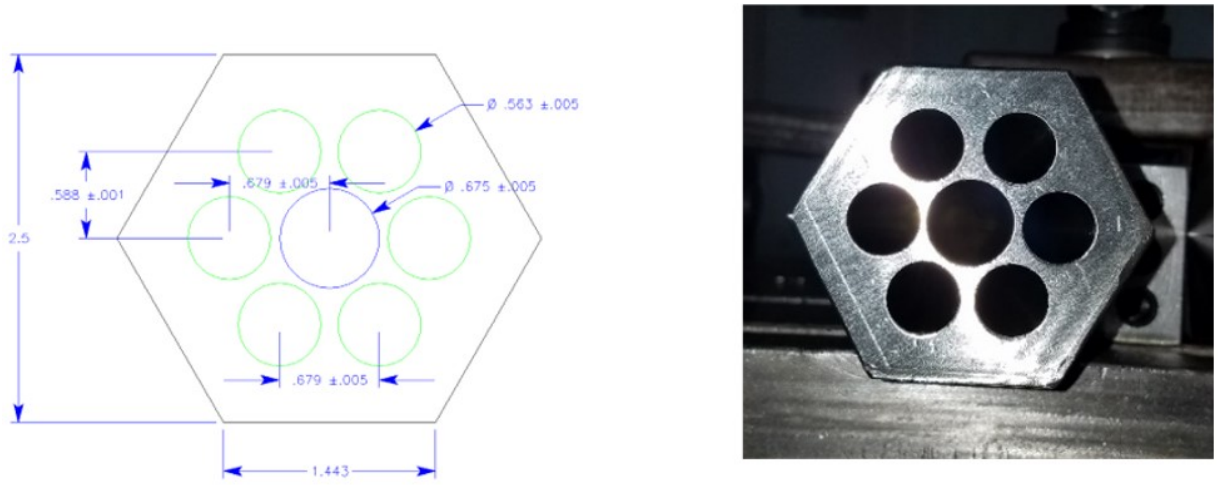

(a) (b)

Figure 5. (a) Cross-section geometry of the core block for single HP experiments. (b) A photograph of a 7-hole hex block end face in fabrication.

Single HP testing is performed in an inert gas environment consisting of either He or an He-Ar mixture. HP assembly is housed in a cylindrical inert gas environment formed by a quartz tube with flanges on either end that include fittings for inlet and outlet gas flows as well as feedthroughs for instrumentation and power. The quartz tube allows for visual observation of heat pipe operation and quantitative thermal imaging. It also provides containment in the unlikely event of a leak of sodium from the HP. As shown in Figure 7, the test chamber is an 8-ft. long, 6-in. diameter quartz tube with flanges for

gas flow connections, instrumentation feedthrough ports, and several internal Macor supports. The Macor ceramic supports are designed to hold the hexagonal core block and the HP centered in the quartz tube. Macor was selected based on its low thermal conductivity and high allowable operating temperature, plus the fact that it is machinable.

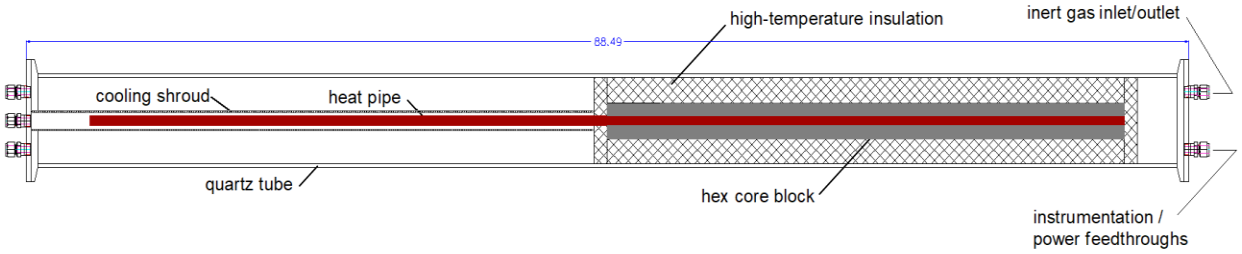

Figure 6. Single HP experiment testbed fixture.

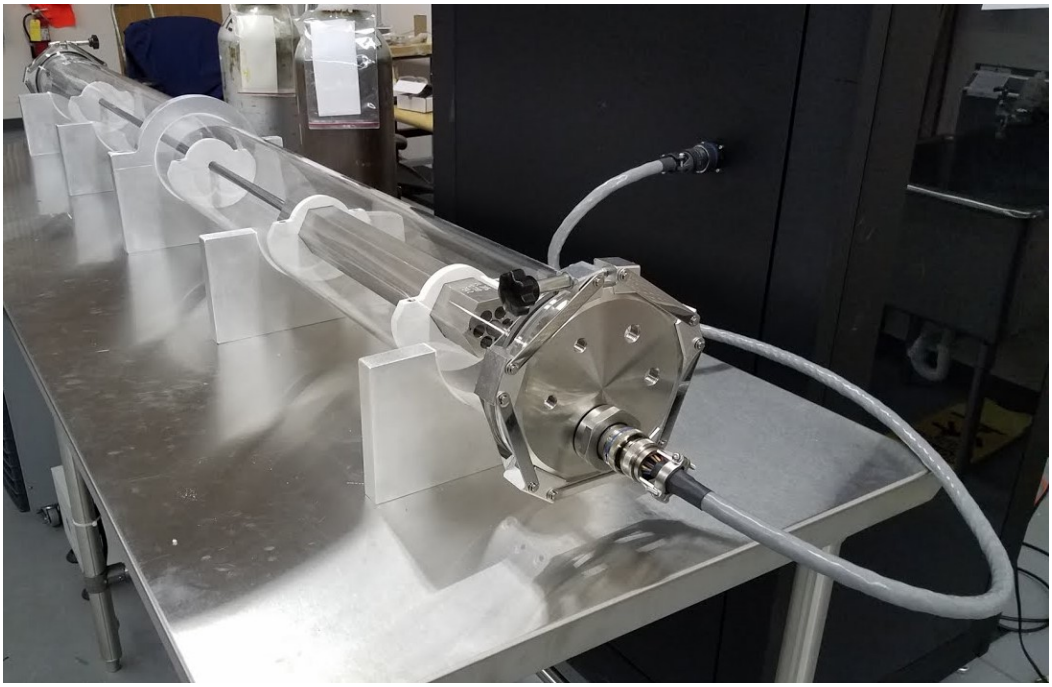

Figure 7. Single HP experiment quartz tube with core block, end flange, and Macor ceramic supports.

The HP is heated with cartridge heaters, which have a maximum heat flux value of 3.8 W/cm^2. This value was selected to mimic the expected microreactor core power densities. Each heater is also interfaced to a LabVIEW virtual instrument. The power supplied to each heater is continuously monitored using precision power meters designed for measurements of silicon-controlled-rectifier (SCR) loads. This is done utilizing Watlow Din-A-Mites SCR-based power controllers.

The initial test article was equipped with a thermowell that allowed for a type-K multipoint thermocouple with ten points to be used to get internal temperature measurements along the axis of the HP. External thermocouples, also type-K, were spot-welded to the outside of the HP, as well as on the outside of the hex block, using stainless-steel straps to get a better temperature distribution of both the HP and the hex block. For future experimental tests, strain gauges will be installed to get an accurate measurement of stress on both the HP and hex block. All the instruments will be interfaced to a LabVIEW virtual instrument processor for data acquisition and instrument control.

3.2 MAGNET Facility

To support the development of microreactor technology, INL has established a 250-kW electrically heated microreactor test bed to enable experimental evaluation of a variety of microreactor concepts. MAGNET was constructed at INL to assist in the development, demonstration, and validation of microreactor components and systems. The purpose of this test bed is to support technology maturation that will reduce uncertainty and risk relative to the operation and deployment of this unique class of systems. However, the testbed will be constructed to accommodate other designs in addition to HP-cooled reactors. MAGNET was constructed at INL with the following objectives and technical goals:

- Provide displacement and temperature data that could be used to verify potential design performance and to validate accompanying analytical models.
- Show structural integrity of core structures (e.g., thermal stress, strain, aging/fatigue, creep, deformation).
- Evaluate the interface between the HPs and HX for both geometric compatibility, HP functionality, and heat transfer capabilities.
- Develop potential high-performance, integral HXs based on advanced-manufacturing techniques, incorporating high-efficiency heat transfer from the HPs or gas working fluid to the power conversion unit (PCU).
- Test the interface between the HX and integrated systems for power generation or process-heat applications.
- Test microreactor components, such as gas circulators, control drums, or heat sinks.
- Demonstrate the applicability of advanced fabrication techniques, such as additive manufacturing or diffusion bonding, to nuclear reactor applications.
- Identify and develop advanced sensors and power conversion equipment, including instrumentation for autonomous operation.
- Test waste heat recovery systems designed to increase system efficiency and improve economics.
- Study cyclic loading and simulated reactivity feedback.
- Enhance readiness of the public stakeholders—particularly DOE laboratories and the NRC—to design, operate, and test new types of high-temperature reactor components.
- Capture data relevant to the development of autonomous microreactor structural integrity monitoring systems, such as digital image correlation (DIC). Use the data to develop and verify models and systems for system-integrity monitoring.

A process flow diagram of MAGNET and a graphic of the MAGNET environmental chamber are shown in Figure 8. The design specifications for MAGNET are shown in Table 1.

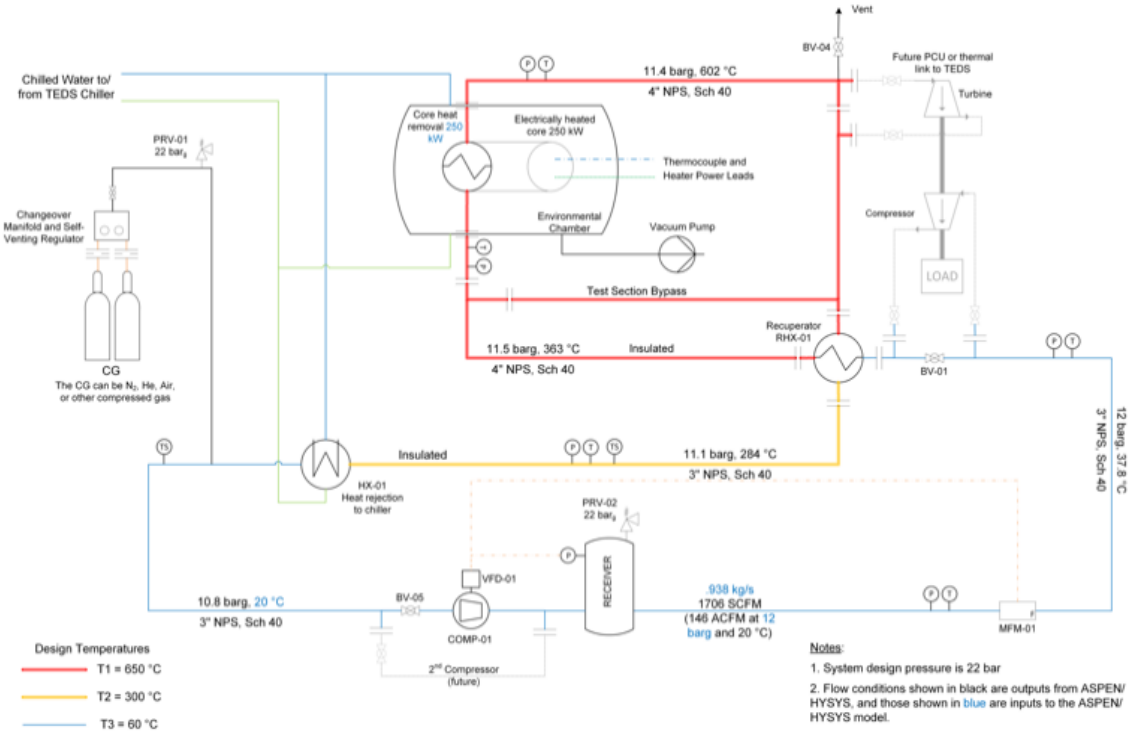

(a)

(b)

Figure 8. (a) MAGNET process flow diagram. (b) MAGNET environmental enclosure.

Table 1. MAGNET facility design specifications.

Parameter	Specifications and Values
Chamber Size	5 ft × 5 ft × 10 ft
Heat Removal	Liquid-cooled chamber walls, gas flow
Coolants	Air, inert gas (He or N_2)
Gas Flowrate	Up to 43.7 ACFM at 290 psig
Design Pressure	22 barg
Maximum Power	250 kW
Max. Temperature	750°C
Heat Removal	Passive radiation or water-cooled gas-gap calorimeter

To provide capabilities for integrated power conversion testing, a modified, commercially available Capstone C30 microturbine unit [21] has been acquired, as observed previously in Figure 8, and will be integrated with MAGNET. Figure 9 shows the key components of the PCU, including the compressor, turbine, alternator, internal recuperator, gas cooler, and power management and distribution (PMAD) subsystem. The generated power can be fed to the electrical heaters in MAGNET to supplement externally supplied electricity or to a load bank as part of the co-located Microgrid Research Laboratory. The cycle is completely closed, and gas flows through the compressor and recuperator into the heat-source HX, into the turbine, back into the recuperator, and finally into the gas cooler for the rejection of waste heat.

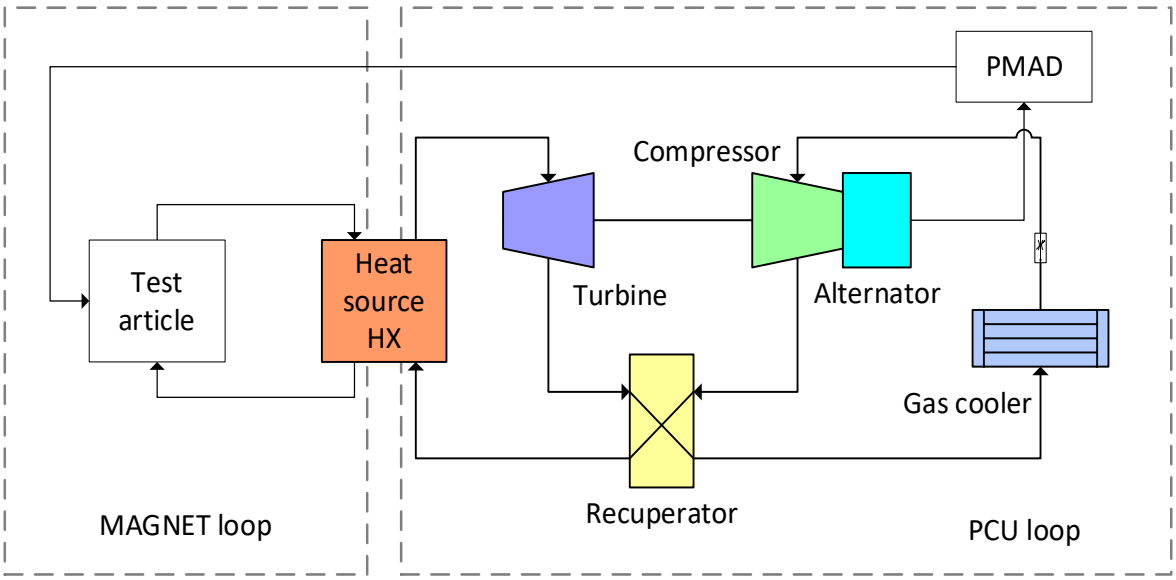

Figure 9. Layout of PCU loop connected to the MAGNET loop by the heat-source HX.

The C30 recuperator is an annular gas-gas HX that is physically integrated within the PCU housing, whereas the heat-source HX can be a gas-gas or liquid-gas HX, depending on reactor design. This PCU has been modified to use electrical heating [22], rather than fossil-fuel combustion, to provide a maximum power output of ~30 kWe in a closed Brayton cycle (CBC) loop with nitrogen as the working fluid. A detailed PCU description and integration into MAGNET is given in Ref. [23]. A proposed set of tests of the power-control schemes and heat-source/PCU coupling are outlined in Ref. [24].

3.3 Advanced Manufacturing Capabilities

Advanced manufacturing (AM) has introduced new techniques for novel design, fabrication, and instrumentation of HPs. The versatility of AM compared to traditional subtractive manufacturing techniques can address heat pipe challenges such as manufacturing unique geometries, complex porous wick structures, pore size and distribution, permeability thickness, thermal contact with chassis, sealing the casing and wick structures, and reduction in material, cost, and time for production of low volume components [25]. Preliminary investigations at INL of heat pipe design using digital light photoluminescence have demonstrated the capability to combine the porous wick and solid region within one component, optimization of internal pore structure and highlight the importance of digital light photoluminescence (DLP) printing and sintering parameters [26]. Additionally, the flexibility of AM's layer-by-layer deposition and process control offers a novel avenue for which sensors and instrumentation can be integrated into the structural design.

Recently with the high demand for real-time data collection to enable process and operational monitoring with data analytics, interest has grown in AM components with sensors embedded within the structures during the manufacturing process, also known as smart manufacturing or smart-enabled components [27]. In heat pipes, measurements of temperature, pressure, and strain in probe locations of interest such as wick structures, which are not achievable without integrated sensors can become viable with AM. Researchers have demonstrated that even wireless communication sensors such as acoustic wave temperature sensors can be successfully printed into components and maintain functionality [28]. Fiber-optic strain sensors embedded in a HP chassis using AM has also been performed and can be found in detailed in Section 4.2.1. While AM-integrated sensing methods are emerging, literature still lacks performance data of these components in harsh conditions such as high-temperature and corrosive environments. New strategies and techniques utilizing AM should be further explored for HP design, instrumentation, and experimentation within SPHERE and MAGNET facilities which can enable further insight and improvements in overall HP operation and performance. A list of some AM methods available at INL and a brief description can be found below:

- Laser engineered net shaping (LENS^{TM}): A blown powder-based directed energy deposition (DED) method which allows for in-situ spatial multi-material composition control.
- Digital light photoluminescence (DLP): A photopolymer resin-based method like binder jet which allows highly complex geometries printed a green part and requires deboning and sintering for final part.
- Wire-arc additive manufacturing (WAAM): Gas tungsten arc-welding method with high deposition efficiency and excellent for large-scale structures.
- Laser powder bed fusion (LPBF): A powder-bed DED method which provides a self-supported bed allowing for complex geometries with porous and lattice structures.

4. INVESTIGATION OF ADVANCED MEASUREMENT TECHNIQUES

After the extensive literature review, this section provides the possible advanced measurement techniques that can be applied for the high-temperature HP experiments with SPHERE and MAGNET facilities at INL. The available techniques are summarized and outlined in the category of measuring parameters of interest.

4.1 Temperature Measurement

To determine the HP thermal performance, temperature measurement is a key parameter to investigate. For the alkali metal charged HP, the resultant high-temperature and corrosive environment limit the available component and instrument material options. Traditional temperature measurement techniques, such as thermocouples, offer excellent compatibility and reliability, but are not scalable to provide high-density measurements suitable for computational fluid dynamic code validation. Although it will be quite tricky to get the temperature data inside the operating high-temperature HP, there are still some available techniques for measuring the external and internal temperature distribution of the HP during operation.

4.1.1 Thermal Imaging Camera

As a non-contact and non-intrusive measurement device, the thermal imaging camera detects the infrared energy emitted, transmitted, or reflected by all materials and converts the energy factor into a temperature reading or thermogram. As an example, Figure 10 demonstrates the temperature profiles measured on the outer surface of the HPs using the thermal imaging camera. Because this still involves traditional optic imaging methods, there are certain limitations for high-temperature applications, including the emissivity variation with temperature, reflection from surfaces, etc.

Figure 10. Video snapshot with a thermal imaging camera filming the HP in use. Adapted from [29].

Since this thermal imaging technique requires a visualization of the test article during the whole measuring process, it is a must to have optical transparency between the camera and the object of interest. Because the SPHERE facility, as shown in Figure 7, has the capability to grant optical access with the quartz tube containing the test article, the thermal imaging camera was utilized during the SPHERE facility shakedown test. [20] As shown in Figure 11, the sodium-charged HP was located in the center of the hexblock, surrounded by six cartridge heaters. Due to the concern of significant radiation heat loss when exposing the heated components, the thermal imaging camera is utilized to verify the surface temperature measurements.

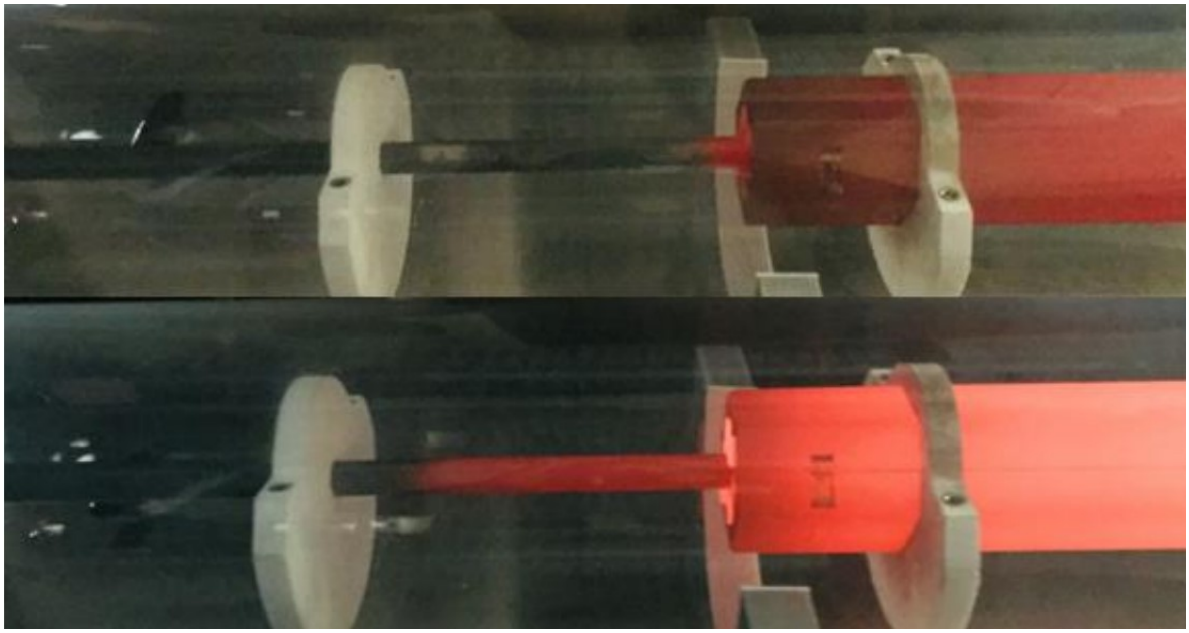

Figure 11. Optical image from the digital camera of the SPHERE shakedown test during the heating process. The HP was located in the center of the hexblock, surrounded by six cartridge heaters.

4.1.2 Distributed Temperature Sensor using Fiber-Optic

As a relatively new technique, distributed temperature sensing using fiber-optic is based on Rayleigh scattering and swept-wavelength interferometry, thousands of temperature measurements can be acquired along a single optical fiber [30]. The scheme and principle of the distributed temperature sensing system is illustrated in Figure 12. A random distribution of impurities and structural variations along the fiber core gives rise to a backscatter pattern that is unique to the fiber and generally stable. The spectrum and amplitude of this pattern can be read to serve as a fiber signature. Given the mentioned advantage, a distributed temperature sensor (DTS) can span large flow fields and function in environments that are unsuitable for image-based techniques [31]. With the improved coating formula and protection, the DTSs have been shown to function well at temperatures up to 600°C [32]. As a recent progress, Gerardi et al. [33] immersed their improved DTSs in a liquid sodium pool and obtained high-resolution liquid sodium temperature measurements.

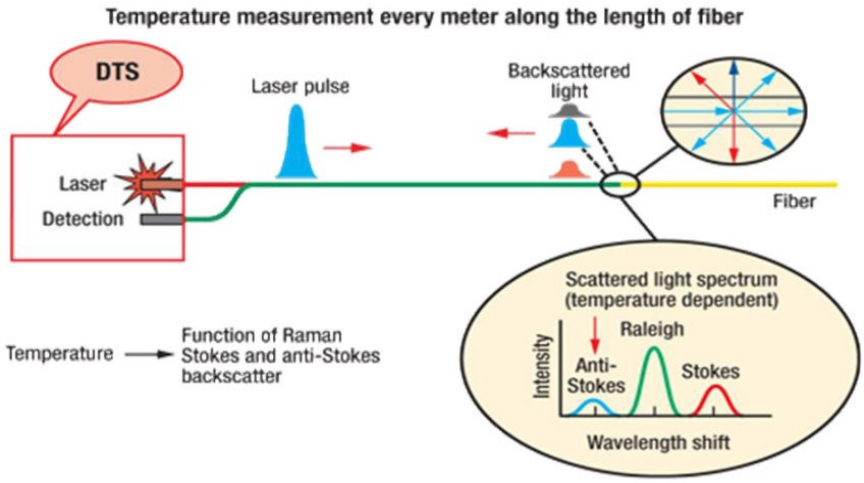

Figure 12. The principle of distributed temperature sensing using fiber-optics. Adapted from [34].

4.2 Stress/Strain Measurement

To assure the accuracy of the stress measurements, the traditional strain gauges will usually need to be welded onto the test object. As an intrusive method, this will affect the structural integrity of the test article, especially for high-temperature test conditions. For example, as for an American Society of Mechanical Engineers (ASME) stamped pressure vessel, it is not allowed to spot-weld any strain gauges to it after receipt. Therefore, some practical advanced measurement methods are introduced in this section for the stress/strain investigations.

4.2.1 Embedded Fiber-Optics

The ability to embed sensors such as fiber-optics, which can provide spatially distributed temperature and strain measurements within microreactor components for real-time health monitoring, would be particularly advantageous. Recent advances in AM method of ultrasonic additive manufacturing (UAM) have demonstrated the successful embedding of fiber-optics in soft materials, such as aluminum (Al) and copper (Cu), by placing the sensors in machined cavities and ultrasonically welding over the top with thin foils. In UAM, material is additively built through a sheet lamination process by welding together thin metal foils through a combination of downward applied force and lateral scrubbing at ultrasonic frequencies, as shown in Figure 13.

Leading the research group at Oak Ridge National Laboratory (ORNL) in 2019, Petrie et al. [35] used UAM to embed fiber-optic strain sensors on top of a stainless-steel 304 (SS304) base with multiple nickel (Ni) layers, relying on the severe plastic deformation of Ni around the fiber to achieve strain coupling to the SS304 base. Differential thermal strains were accurately monitored along the length of the embedded fiber at temperatures approaching 350°C before the fibers mechanically failed. The potential failure reason could be that the difference in thermal expansion coefficients between SS304 and pure Ni could result in delamination between the Ni foils and the SS304 matrix at higher temperatures. Based on this experience, for the first time, Hyer et al. [36] proposed a new method to investigate the processing and microstructure of UAM-fabricated SS304 foils to a SS304 base while simultaneously embedding fiber-optic sensors in the metal matrix, as shown in Figure 14. The UAM processing parameters and foil materials were first varied by using SS304 plates. Select plates were sectioned for microscopy to establish the effects of the processing conditions on the embedding process. Fiber-optic sensors were then successfully embedded within the SS304 test articles, including a pipe and a hexagonal component representing a section of an HP–based microreactor core block, as illustrated in Figure 14. Temperature and strain monitoring of the pipe test article were subsequently performed by using optical frequency domain reflectometry (OFDR) during electrical heating to demonstrate the potential for spatially distributed health monitoring during microreactor operation. Due to the high operating temperature, there could be some difficulties to distinguish the temperature effects from the strain effects, which will need to be investigated and quantified as future work.

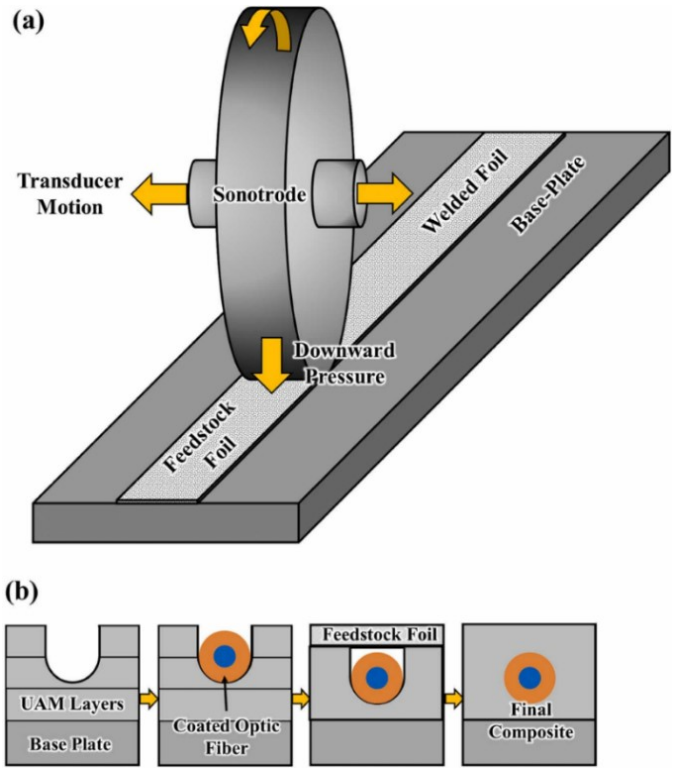

Figure 13. Schematic representations of the (a) UAM process and (b) fiber embedding steps (section view), which include building a few layers of material on the baseplate, machining a channel, laying the fiber-optic in the channel, and layering foils on top to embed the fiber. Adapted from [37].

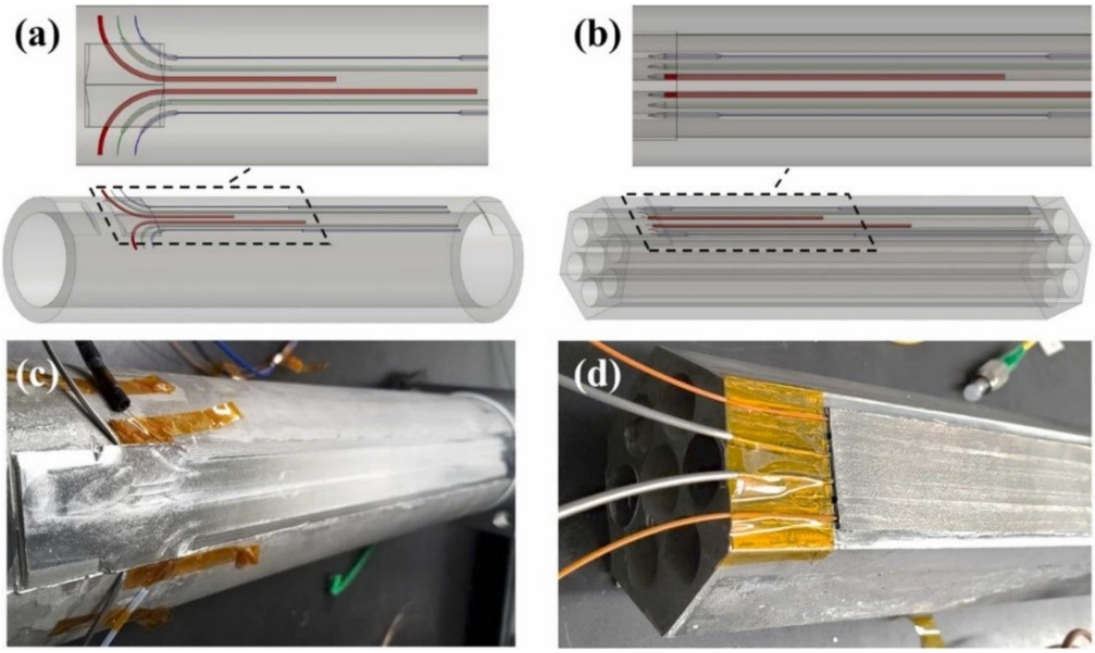

Figure 14. CAD models (a, b) and pictures (c, d) of the pipe (a, c) and hexagonal block (b, d) test articles with embedded thermocouples and fiber-optic sensors. The thick red lines correspond to the location of the thermocouples, the thin green lines designate the placements of the fiber-optics, and the thin blue lines indicate open cavities for insertion of a floating fiber. Adapted from [36].

4.2.2 Digital Image Correlation

In addition to fiber-optic strain sensors, there is one more option known as DIC that can be implemented for the SPHERE and MAGNET facility. DIC is a technique that may prove to be ideally suited for the study of crack propagation and material deformation in real-world applications, as it has the potential to become a less expensive, simple and yet accurate [38]. However, optic access like the quartz tube containment in SPHERE is a must to allow for the use of the non-contact DIC technique for characterizing local strains. DIC involves the use of one or more imagers for measuring deformation of structures; therefore, it can achieve sub-pixel resolution. This makes it attractive in applications that allow for line-of-sight viewing of the structure of interest because they allow the capture of deformation information with a very high spatial resolution.

Having the capability to perform measurements at high-temperature test objects, DIC has shown itself to be a very attractive technique for measuring strain and deformation at high spatial resolution as a non-contact, imager-based technique that can potentially be used to measure strain and deformation in two or three dimensions. In a typical DIC measurement, a speckle pattern is applied to the structure being tested and is observed as it undergoes deformation loading using imagers [39]. In the case of the microreactor core block, the speckle pattern will be applied to the test article using high-temperature paint. Similar to the setup for SPHERE, INL's MAGNET facility has optical windows that can provide required optical access for DIC, which can measure the full-field deformation of the core block, along with all other embedded and spatially distributed sensors that can be deployed within the MAGNET experiments. It is important to match the size of the random speckles such that they take up roughly 5–10 pixels in the image plane to maximize spatial resolution. The research team [40] supporting MRP is currently making use of computer graphics simulations, as shown in Figure 15, to estimate the proper size of the speckle pattern given the MAGNET facility viewport locations that can accommodate the imagers.

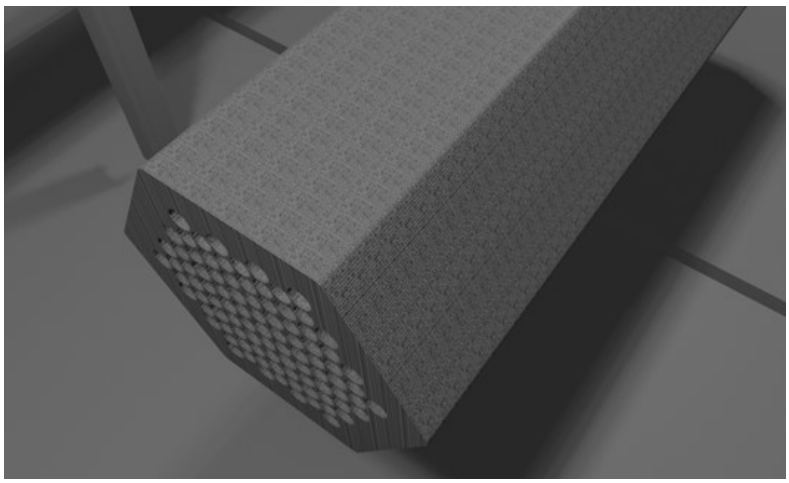

Figure 15. Simulation of 37-hole core block with speckle pattern for the MAGNET facility.

4.3 Void Fraction and Film Thickness Measurement

To model the HP with computational tools and predict its thermal behavior, the phase change physics with the alkali metal charged in the HP is one of the most essential and crucial pieces—especially during the HP transient scenarios (e.g., the starting and cooling phases). Even if there are available computational software and models to deal with the phase change problems, like STAR-CCM+ and MOOSE (Sockeye), the V&V efforts are inevitable and indispensable when dealing with the high-temperature HP systems. Therefore, it will require the high-fidelity experimental database for the operating HPs, and the void fraction measurement to support V&V effort.

4.3.1 Optical Measurement with High-Speed Camera

Based on a traditional optical measurement with high-speed cameras, it is possible that researchers can visualize the inside of an operating HP. However, this measurement technique does have limitations to consider when designing the experiment facilities. Unlike SPHERE and MAGNET, which are designed to conduct high-temperature liquid metal HP experiments, Shi et al. [41] proposed and designed a Low-Temperature Heat Pipe Test Facility (LTHPF) to develop a more detailed experimental database, including internal measurements and flow visualizations. It was demonstrated previously that scaling laws can be used to study high-temperature HPs using low-temperature test facilities [42], where the similarity laws were derived directly from governing equations and constitutive relations using the modeling framework developed by Shi et al. [43]. Figure 16 shows the LTHPF before the insulation. Utilizing intrusive measuring techniques, the adiabatic section comprising of an instrumentation port, where liquid film thickness, temperature, and pressure measurements can be taken, in addition to a visualization port. The visualization port is comprised of a sight flow indicator with two stainless-steel flanges and a borosilicate glass tubing. The section is insulated except for the sight glass of the port. The HP experiments using LTHPF are still undergoing preliminary tests; therefore, the detailed instrument setup, including all measurement uncertainties, will be made available when more experimental data becomes available.

Figure 16. The LTHPF at the Thermal-Hydraulic Laboratory led by Prof. Shanbin Shi from Rensselaer Polytechnic Institute (RPI). Adapted from [44].

4.3.2 Heat Pipe Visualization

The visualization of the heat pipe was performed at Texas A&M University (TAMU). Complex phenomena that occur inside of the heat pipe corresponding to the external condition of the operation are one of the largest concerns for modeling the overall thermal-hydraulic behavior of heat pipes. As the first milestone of heat pipe visualization, TAMU performed heat pipe construction and experiment using a water heat pipe. Later, works will be extended to the sodium heat pipe. The construction of the heat pipe was conducted using a transparent glass tube. The evaporator region of the heat pipe was coated by a clear glass heater and the condenser region has a cooling jacket made of the acrylic tube. As a result, the entire heat pipe is made transparent, allowing for visualization of the heat pipe's interior phenomena. The thermal-hydraulic behavior of the heat pipe was visually collected by high-speed cameras and infrared (IR) cameras and analyzed.

The external surface temperature of the heat pipe is a result of complex phenomena inside of the heat pipe and typically has been used as a validation set of data for heat pipe modeling. The application of an IR camera to heat pipe research is beneficial not only due to the field-wise temperature information it provides but also clear insights to understand the thermal behavior of heat pipes. Figure 17 shows some examples of IR images obtained during the operation of the heat pipe. As shown on the left side, the propagation of the heat from the evaporator to the condenser can be easily recognized when the outer surface of the whole heat pipe is captured using the IR camera. The behavior of the heat pipe at the onset of operating limitation also can be investigated using the IR camera, as shown on the right side of the figure. Especially when the phenomenon of the fluids inside of the heat pipe is visualized simultaneously, some insights to understand the evolution of the operating limitation might be achievable. This visualization of the heat pipe using the IR camera and high-speed camera has been performed at TAMU.

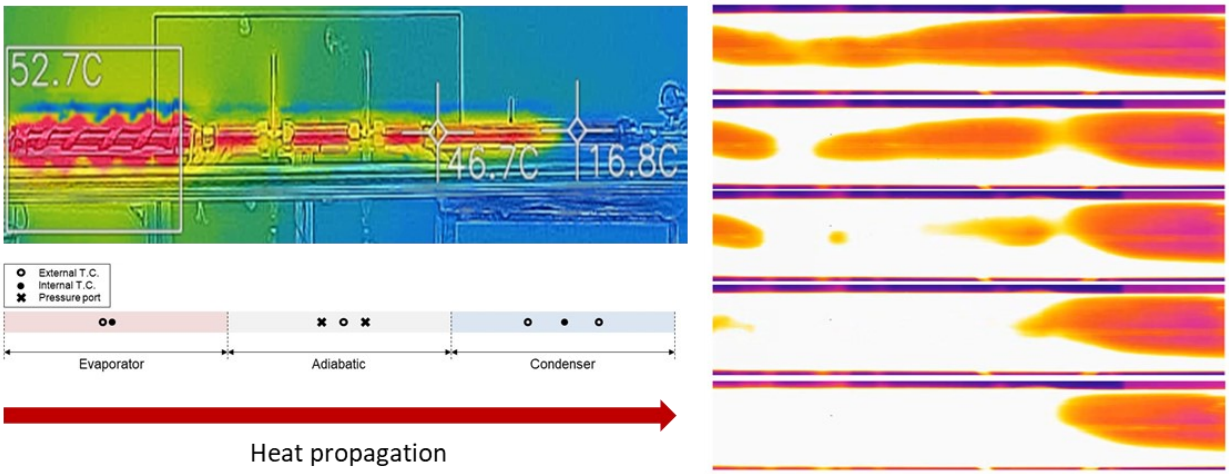

Figure 17. Temperature measurement of IR camera for heat propagation (left) and operating limitation of heat pipes.

Figure 18 shows the picture of the heat pipe visualization experimental setup. The experimental setup consists of three parts, the heat pipe, the heating & cooling regions, and the measurement system. A heat pipe with an annular wick was constructed. To fabricate the wick structure, mesh screens were wrapped around a 1.2 m long rod with a diameter of 17 mm, then spot welded to retain the cylindrical shape along the axial direction with 1.5 ~ 2.0 mm intervals. After removing the rod, the wick structure was inserted into a 1.2 m borosilicate seamless glass tube pipe with an outer and inner diameter of 25.4 mm and 19.9 mm, respectively. The dimensions of the manufactured screen mesh are 18.8 mm of inner diameter, 0.49

mm of thickness, and 19.29 mm of outer diameter. Construction of heat pipe consists of cleaning, vacuuming, fluid filling, and sealing processes. The glass tube and wick structure were thoroughly cleaned using ethanol and acetone. Each end of the pipe was closed using compression fittings. One side of the pipe was connected to the vacuum pump and working fluid filling system. After -90 kPa of vacuum pressure was achieved by the vacuum pump, 240 mL of deionized water was inserted into the pipe as a working fluid. Then, the pipe was sealed by a locking ball valve connected to the vacuum pump. As a final step of the fabrication, leakage was checked to verify the condition inside the heat pipe. The fabricated heat pipe with an annular multi-layered screen mesh was then fixed with a horizontal geometry. A transparent heater, the evaporator section of the heat pipe, was connected to a direct current (DC) power supply with a maximum output of 3 kW. A water jacket was installed at the condensing region of the heat pipe to remove the heat transferred by the heat pipe. The inlet temperature of the cooling fluid inside the water jacket was controlled by a Merilin M33 chiller from the Neslab company. To examine the boiling phenomenon and fluid flow in the heater more precisely, high-speed cameras are mounted at the top and bottom. An infrared camera is installed at the bottom to monitor the temperature change of the heater. Because this experiment emphasizes visual observation of the heat pipe's interior phenomena rather than thermal or hydrodynamic analyses, we concentrated on establishing observation equipment capable of viewing this well and did not apply any insulation.

As shown on the right side of Figure 18, the flow of fluid inside the heat pipe was visually observed in this experiment. In particular, the boiling phenomena occurring in the evaporator section and the temperature change associated with it were primarily monitored. Various patterns of boiling were observed, and rapid behaviors of phase change were captured by a high-speed camera. Local temperature information achieved using the IR camera was compared with the local phenomenon. At a higher power range, internal phenomena during the progress of operating limitation were captured, and corresponding changes in surface temperature was investigated. It was found that the distribution of the liquid at the gap of the annular heat pipe is a primary factor for the external temperature distribution, and the interval of the large-scaled boiling, Geyser boiling, for example, is also an important factor.

As a further study, TAMU is planning to apply frequency based image analysis, and perform multiple sets of experiments with expanded boundary conditions to correlate external temperature and internal phenomena.

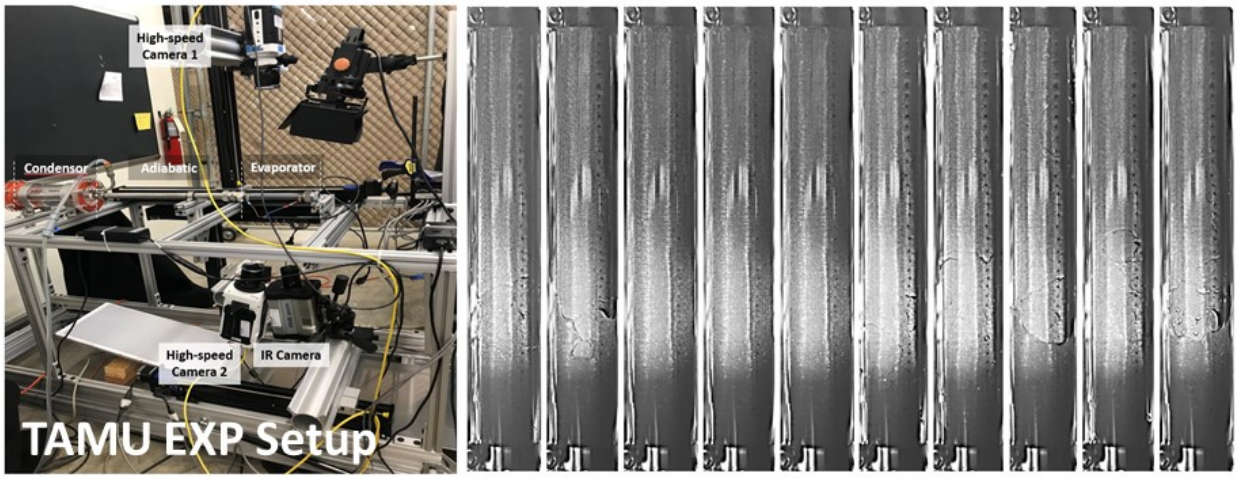

Figure 18. TAMU Experimental setup of the heat pipe visualization experiment (left), and an example of fluid flow inside of the heat pipe captured by high speed camera with 100W input power, 0 degree inclination, 2000 fps of camera frame rate (right).

4.3.3 Radiation-based Tomography

As supervised by Prof. Annalisa Manera and Dr. Victor Petrov, a state-of-the-art sodium-filled HP experimental facility termed MISOH1 was designed and constructed to generate high-fidelity experimental data at the University of Michigan (UM). The research investigates the HP startup process and its performance under various operation conditions, including the effects of the heat transfer rate, the cooling condition of the condenser section, and HP orientation. Figure 19 shows the schematic diagram of the test facility. The test section assembly consists of an evaporator (254 mm), an adiabatic (508 mm), and a condenser (254 mm) section, respectively. At the evaporator section, the silicon carbide (SiC) double spiral heater—consisting of a 52 mm outer diameter, a 40 mm inner diameter, and a 254 mm heating length—was installed concentrically with the HP to supply heat through a radiational heat transfer. The heater can be used within the maximum power of 4,500 W and a maximum continuous operating temperature of 1200°C. The material of the heater was selected with the consideration of a low Z-number to reduce the attenuation of X-rays for the radiography measurement.

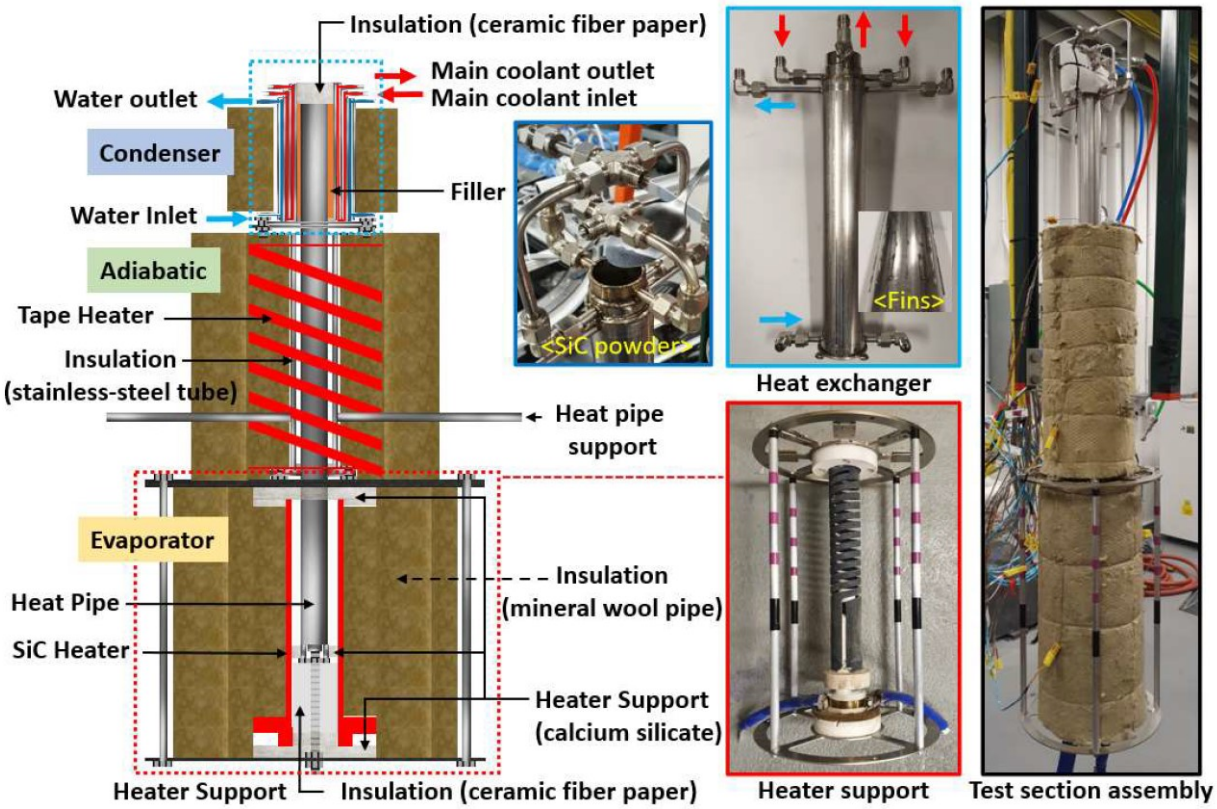

Figure 19. Schematic diagram of a separate-effect test facility for a single sodium HP. Adapted from [45].

A high-speed X-ray radiography system was applied to observe the two-phase flow phenomena inside the sodium HP during startup operation. Figure 20 shows the schematic diagram of the X-ray radiography system. It is comprised of an X-ray generator (max. voltage: 150 kV and max. current: 400 mA), a cadmium telluride (CdTe) detector, and a control system. As the working principle of the radiation attenuation measurement, the photons emitted by the radioactive X-ray tube source are attenuated or absorbed as they travel through various materials of the object. The intensity of the attenuated radiation is then measured by the detector located on the opposite side of the test section, as illustrated in Figure 20.

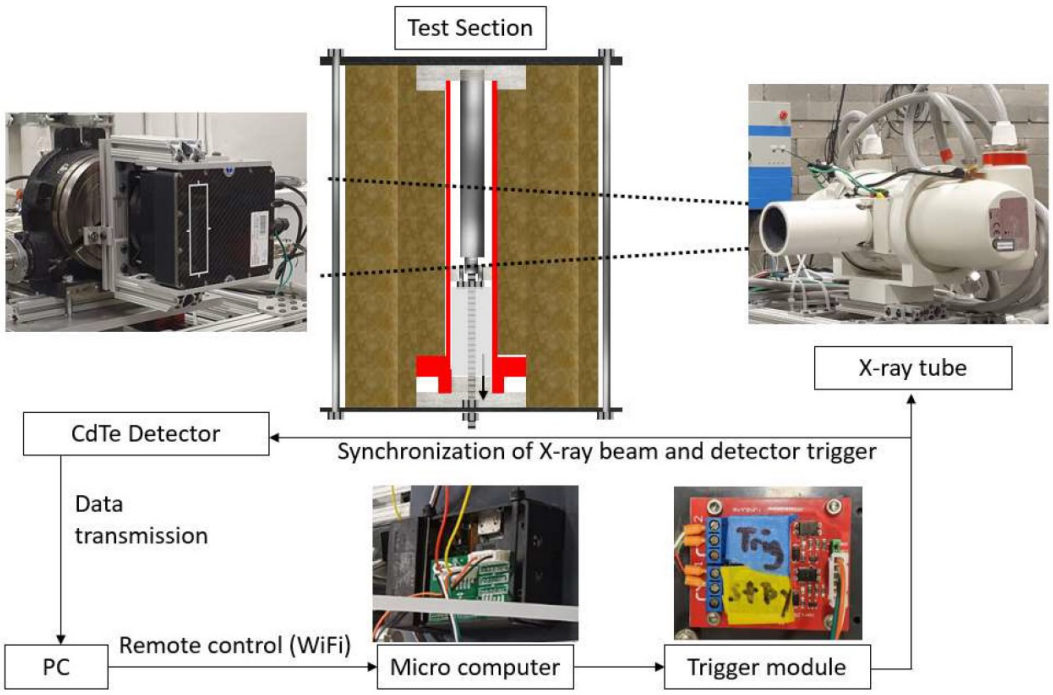

Figure 20. The schematic diagram of the X-ray radiography system. Adapted from [45].

As a successful demonstration of the operating HP visualization by the UM research group, Figure 21 shows eight X-ray snapshots at pre-selected times during the startup process. The images were taken at the lower region (e.g., 0 –100 mm) of the HP evaporator. The area in blue on the images indicates strong x-ray attenuation; on the other hand, the area in red indicates weak x-ray attenuation. The stainless-steel end cap of the HP is presented at the bottom of the images with strong attenuation, and moved down due to the thermal expansion of the HP during the heating process. The stripe patterns on the background represent the projection of the SiC heater that was not completely removed in the calibration process.

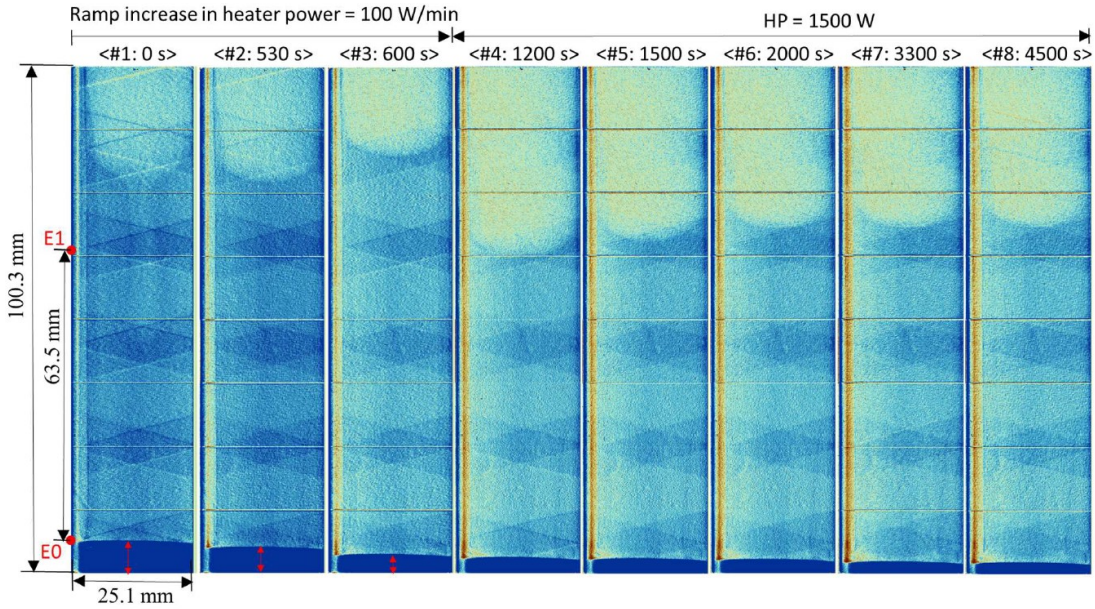

Figure 21. X-ray images of two-phase flow in the evaporator section of the HP. Adapted from [45].

4.3.4 Radiation Diagnostics with Sodium Isotope (Na-22)

Besides the radiation-based tomography, there is another way to utilize the radiation method for visualization inside a certain structure, which is known as a radionuclide scan for medical use. A radionuclide scan is an imaging technique that uses a small dose of a radioactive isotope called a 'tracer' that can detect cancer, trauma, infection, or other disorders [46].

Inspired by this technique with radioactive isotopes, an innovative idea can be proposed to customize a dummy sodium (Na)-charged HP with an Na radioactive isotope known as 'Na-22.' During the HP operation, the characteristic 511 keV photon, as shown in Figure 22, can be detected whenever Na-22 emits positrons as part of its decay process. With the radiation detector, the count density will provide information regarding the sodium distributions as a sodium-charged HP operates. However, due to the limited information reported in the literature, this is still a preliminary hypothesis, and how practical this method will turn out to be will still need to be examined and verified as future work.

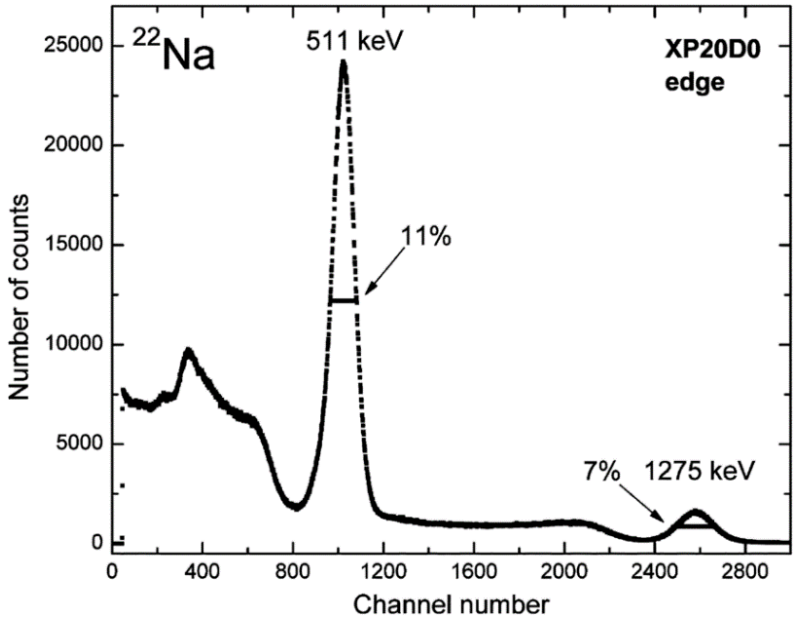

Figure 22. The energy spectrum of gamma rays from an Na source. Adapted from [47].

4.4 Advanced Laser Spectroscopy for Velocimetry, Pressure, and Temperature Measurement inside an HP

Based on recent investigations, Prof. Philippe Bardet from the George Washington University (GWU) has proposed utilizing laser spectroscopy to measure the temperature, pressure, and velocity of the vapor region within a sodium-charged HP. Prof. Bardet has used similar techniques in water vapor for High-Temperature Gas-cooled Reactor (HTGR) in the past.

Sodium vapor spectrum is well known, and the sodium characteristic D-line is even a common calibration light source. It offers a few diagnostic routes to directly probe the gas with laser-matter interaction principles. While more refined and sophisticated to deploy, such techniques offer tremendous advantages over traditional probe approaches. They are non-intrusive, of dynamic order 0 (i.e. their response is instantaneous), uncertainty analysis is readily traceable. Figure 23 shows the energy levels of Sodium vapor. The main two D-lines correspond to visible light spectrum and are the reason for the nice yellow glow of sodium lights. There are a broad range of lasers that operate near these wavelengths (other transitions can be probed as well), and Figure 24 shows a laser in resonance with sodium in a gas cell.

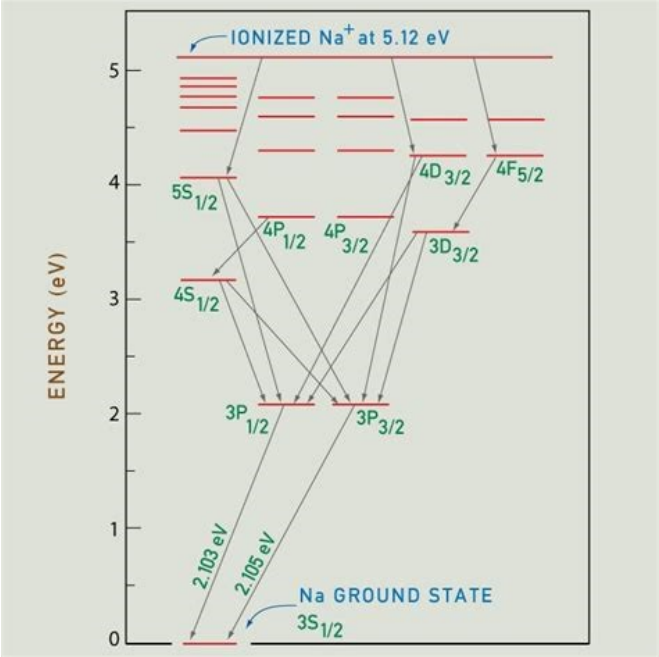

Figure 23. Sodium energy levels: the transitions 3P1/2-3S1/2 & 3P3/2-3S1/2 corresponds to the sodium D-lines at λ=589.6 & 589.0 nm, respectively.

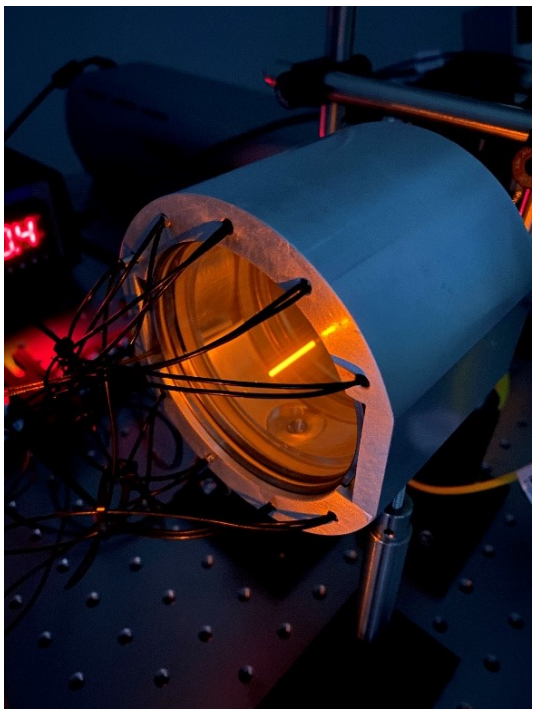

Figure 24. Tunable laser being absorbed in resonance with sodium in a gas cell. The orange line marks the laser path. (Courtesy Dr. Michael Button, who developed TDLAS during his PhD with Dr. Bardet.)

The two main approaches that could be considered for measurements of velocity, temperature, and pressure are tunable diode laser absorption spectroscopy (TDLAS) or laser induced fluorescence (LIF). For the sake of conciseness, principles of TDLAS are briefly described here.

TDLAS relies on Beer-Lambert law of absorbance, which relates laser beam attenuation to the system dimensions, gas composition, pressure, and temperature:

$$\tau_\nu = \left(\frac{I_t}{I_o}\right)_\nu = \exp(-\alpha_\nu) \quad (1)$$

where τ_ν is the transmittance of laser light, I_t is the transmitted laser intensity, I_o is the incident laser intensity, and α_ν is the spectral absorbance term defined by [48]:

$$\alpha_\nu = P \cdot X_{abs} \cdot S(T) \cdot \phi \cdot L \quad (2)$$

where P is the total pressure (atm), L is the local distance along the beam propagation (cm), X_{abs} is the local mole fraction of the absorbing species, S is the line-strength of the transition (cm^{-2} atm^{-1}), T is the local temperature (K), and ϕ is the line-shape function (cm). The line-strength is a function of temperature alone and relates the fraction of molecules in a given rovibrational state through the partition function, which describes the statistical properties of a system in thermodynamic equilibrium where the states obey a Boltzmann distribution.

Theoretically, the line-shape function of a given absorption transition is derived from the physical interaction between the absorbing species and is dependent on temperature and pressure. The overall line-shape used to model these behaviors is a Voigt profile, which is a convolution of Gaussian and Lorentzian distributions. Gaussian contributions are derived from Doppler broadening, which is caused by the random thermal motion of absorbing molecules. Lorentzian contributions are derived from molecular collisions resulting in broadening and shifting of the linewidth (pressure broadening and shifting). Finally, coherent flow will lead to a Doppler shift of the absorption spectra. With the laser spectrum plotted in terms of the laser signal's intensity versus wavelength, Figure 25 shows the overall principle of technique and how the physical quantities are probed.

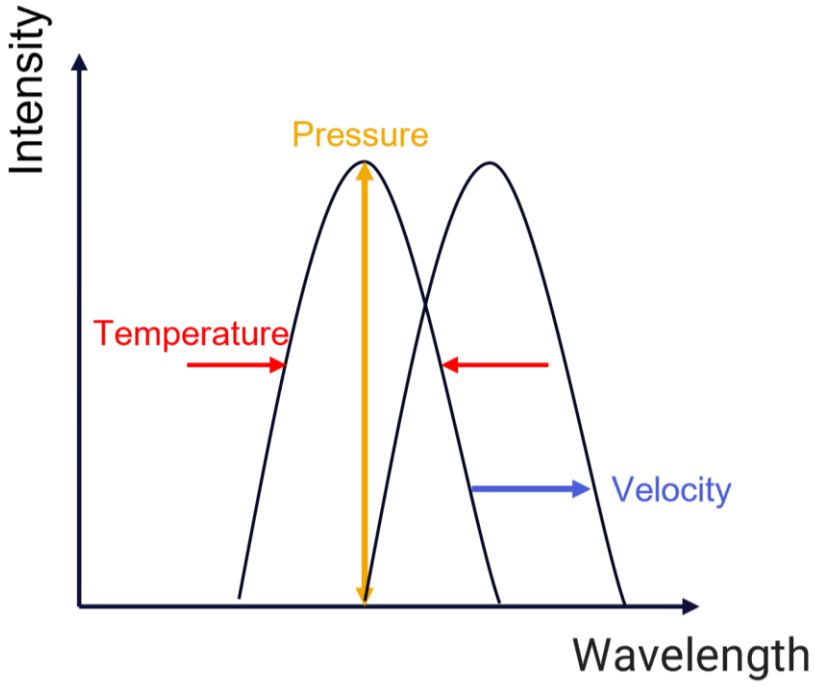

Figure 25. With the angled laser orientation setup, the laser spectrum can be used for post-processing to measure the velocity, pressure, and temperature in the vapor core region.

To apply the TDLAS technique to the internal part of the HP, small through ports estimated to be less than 5 mm in diameter will need to be drilled through the HP wall. As shown in Figure 26, there are two ways to set-up the diagnostic experiments. The straight-on approach, as shown in Figure 26 (a), will fire the laser beam perpendicular with respect to the HP wall. From the opposite side, the laser signal receiver will examine and plot the laser spectrum after it passes through the HP internal vapor core region. In this configuration the sensing is insensitive to Doppler shifting and we will only probe integrated temperature and pressure in the gas core. To reconstruct the absorption peak shape and correlate its shape to Voigt profiles, in TDLAS one scans the laser over a narrow spectral region.

In the second configuration, the laser is to have an angle to capture Doppler shift as well, Figure 26(b). Here two visual ports on the opposite side of the HP wall will allow the incoming laser beam to have an angle with the HP wall. The Doppler shift will be obtained by scanning a fraction of the laser beam through a reference cell (similar setup seen in Figure 24) and the peak location compared. For reference at the speed predicted in the HP, we anticipate a large Doppler shift of nearly one wavenumber, which will make the comparison to the zero-flow (reference) cell very accurate.

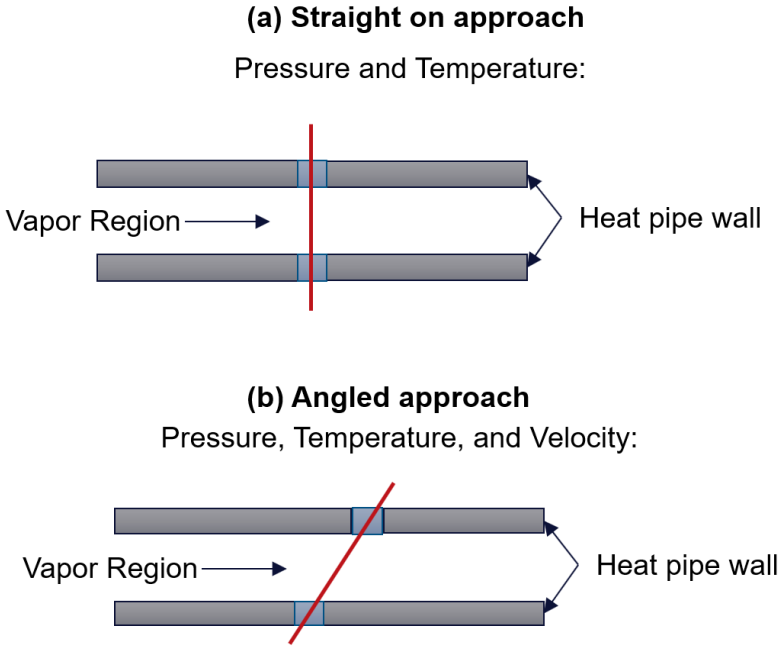

Figure 26. Two different ways to employ the advanced laser diagnostics that can be applied to an operating HP: (a) the straight-on approach with the laser perpendicular to the HP wall; (b) the angled laser orientation with a certain angle to the HP wall.

Overall, this method is based on well-established principles that are actually used to measure gas flow in the troposphere from ground base lasers. While this has not been demonstrated in nuclear applications or heat pipes, we think this technique is quite mature, requires limited resources while achieving the HP internal measurement for velocity, pressure, and temperature at the same time. The main challenge for the deployment of the technique is technical in nature: the design of fiber optics launch inside the heat pipe. From experience in Dr. Bardet's lab, the openings can be as small as 1.25 mm in diameter. To protect the optical elements, diamond coating or diamond anvil cell will need to be applied to the collimation optics. While this sounds expensive, one should keep in mind the small size needed and broad availability of industrial diamonds for diamond anvil cell. Given the balance of the associated benefits and challenges for HP instrumentation, it is worthwhile to investigate this laser diagnostic technique further.

5. SUMMARY AND FUTURE PLAN

An HP-cooled microreactor is among one of the most promising designs that are being actively investigated by the MRP. However, due to the high operating temperature, it is extremely challenging to apply traditional measurement techniques to measure the internal mechanisms of liquid metal HPs when they operate. To gain insights into the HP internal physics, there are some urgent and crucial needs to obtain the variables of interest listed below:

- Temperature on internal and external side of the HP during the full operation cycle
- Stress and displacement measurement for the containment holding the HP
- Internal measurement of void fraction and film thickness for operating HPs
- Vapor velocity in the HP core during operation
- Sodium vapor pressure inside the HPs at different operating stages.

After an extensive literature review, this study summarizes the preliminary investigations of advanced measurement and visualization techniques for high-temperature HP experiments, which can be implemented to support the microreactor research, development, and demonstration (RD&D) process. Advanced manufacturing capabilities have also been examined to support some of these advanced measurement techniques. Innovative techniques are being explored to measure various parameters and support validation needs for high fidelity tools that are being developed under DOE NEAMS program.

Future collaborations with other U.S. research institutes and universities will be considered to examine the feasibility of some advanced HP measurement techniques. The objective of this report is aimed to investigate various advanced measurement and visualization techniques that could potentially be utilized with non-nuclear test beds such as SPHERE and MAGNET. The experimental database that would be generated under the DOE MRP will support and enable accelerated development and demonstration of various microreactor concepts, and assist other DOE programs with V&V effort.

6. REFERENCES

[1] Idaho National Laboratory, "Microreactor Program (MRP) Website, Gateway for Accelerated Innovation in Nuclear (GAIN)." Available: https://gain.inl.gov/SitePages/MicroreactorProgram.aspx (accessed 30 June 2022).

[2] Ge, L., Li, H., Tian, X., Ouyang, Z., Kang, X., Li, D., Shan, J. and Jiang, X., 2022. Improvement and Validation of the System Analysis Model and Code for Heat-Pipe-Cooled Microreactor. *Energies*, vol. 15, no. 7, p.2586. https://doi.org/10.3390/en15072586.

[3] Hansel, J. E., R. A. Berry, D. Andrš, M. S. Kunick, and R. C. Martineau, 2021, "Sockeye: A one-dimensional, two-phase, compressible flow heat pipe application," *Nucl. Technol.,* vol. 207, no. 7, pp. 1096–1117. https://doi.org/10.1080/00295450.2020.1861879.

[4] Permann, C. J., D. R. Gaston, D. Andrš, R. W. Carlsen, F. Kong, A. D. Lindsay, J. M. Miller, J. W. Peterson, A. E. Slaughter, R. H. Stogner, and R. C. Martineau, 2020, "MOOSE: Enabling massively parallel multiphysics simulation," *SoftwareX,* vol. 11, p. 100430. https://doi.org/10.1016/j.softx.2020.100430.

[5] Yoo, J. S., S. Qin, M. Song, J. L. Hartvigsen, Z. D. Sellers, T. J. Morton, P. Sabharwall, J. Hansel, L. Ibarra, B. Feng, and C. M. Petrie, 2021, "Modeling and Analysis Support for High Temperature Single Heat Pipe Experiment: Current Status and Plan," INL/EXT-21-61961, Idaho National Laboratory, Idaho Falls, ID, USA.

[6] Smith, J., R. Singh, M. Hinterberger, and M. Mochizuki, 2018, "Battery thermal management system for electric vehicle using heat pipes," *Int. J. Therm. Sci.,* vol. 134, pp. 517–529. https://doi.org/10.1016/j.ijthermalsci.2018.08.022.

[7] Reay, D. A., 2015, "Thermal energy storage: The role of the heat pipe in performance enhancement," *Int. J. Low Carbon Technol.,* vol. 10, no. 2, pp. 99–109. https://doi.org/10.1093/ijlct/ctv009.

[8] Chaudhry, H. N., B. R. Hughes, and S. A. Ghani, 2012, "A review of heat pipe systems for heat recovery and renewable energy applications," *Renew. Sust. Energ. Rev.,* vol. 16, no. 4, pp. 2249–2259. https://doi.org/10.1016/j.rser.2012.01.038.

[9] Dulera, I. V., A. Basak, P. P. Kelkar, and R. K. Sinha, 2006, "Compact High Temperature Reactor (CHTR)," *BARC NEWSLETTER,* vol. 273, pp. 172–179. Available: https://barc.gov.in/barc_nl/2006/200610.pdf (accessed 30 June 2022).

[10] Panda, K. K., I. V. Dulera, and A. Basak, 2017, "Numerical simulation of high temperature sodium heat pipe for passive heat removal in nuclear reactors," *Nucl. Eng. Des.,* vol. 323, pp. 376–385. https://doi.org/10.1016/j.nucengdes.2017.03.023.

[11] Ranken, W. A., 1982, "Heat pipe development for the SPAR space power system," in *Advances in Heat Pipe Technology*, Elsevier, Amsterdam, Netherlands, pp. 561–574. https://doi.org/10.1016/B978-0-08-027284-9.50055-3.

[12] Dickinson, T. J., 1996, *Performance Analysis of a Liquid Metal Heat Pipe Space Shuttle Experiment*, Storming Media Report Number #A421523, Air Force Institute of Technology, Wright-Patterson Air Force Base, OH, USA.

[13] Reay, D. A., P. A. Kew, and R. J. McGlen, 2014, *Heat Pipes: Theory, Design, and Applications, Sixth Edition*. Butterworth-Heinemann, Oxford, U.K.

[14] Jouhara, H., V. Anastasov, and I. Khamis, 2009, "Potential of heat pipe technology in nuclear seawater desalination," *Desalination,* vol. 249, no. 3, pp. 1055–1061. https://doi.org/10.1016/j.desal.2009.05.019.

[15] Jouhara, H., A. Chauhan, T. Nannou, S. Almahmoud, B. Delpech, and L. C. Wrobel, 2017, "Heat pipe based systems - Advances and applications," *Energy,* vol. 128, pp. 729–754. https://doi.org/10.1016/j.energy.2017.04.028.

[16] Matthews, C., V. Laboure, M. DeHart, J. Hansel, D. Andrš, Y. Wang, J. Ortensi, and R. C. Martineau, 2021, "Coupled multiphysics simulations of heat pipe microreactors using DireWolf," *Nucl. Technol.,* vol. 207, no. 7, pp. 1142–1162.

[17] Hansel, J. E., R. A. Berry, D. Andrš, and R. C. Martineau, 2020, "Sockeye Theory Manual," INL/EXT-19-54395, Idaho National Laboratory, Idaho Falls, ID, USA. Available: https://inldigitallibrary.inl.gov/sites/sti/sti/Sort_27069.pdf (accessed 30 June 2022).

[18] Yoo, J. S., M. Song, S. Qin, and P. Sabharwall, 2022, "A conduction-based heat pipe model for analyzing the entire process of liquid-metal heat pipe startup," in *19th International Topical Meeting on Nuclear Reactor Thermal Hydraulics (NURETH-19)*, Virtual Meeting, 6–11 March 2022. Available: https://www.osti.gov/servlets/purl/1856343 (accessed 30 June 2022).

[19] Qin, S., M. Song, J. S. Yoo, P. Sabharwall, and C. M. Petrie, 2022, "Code-to-code benchmark study for thermal stress modeling and preliminary analysis of the high-temperature single heat pipe experiment," in *19th International Topical Meeting on Nuclear Reactor Thermal Hydraulics (NURETH-19)*, Virtual Meeting, 6–11 March 2022. Available: https://www.osti.gov/servlets/purl/1847912 (accessed 30 June 2022).

[20] Sabharwall, P., J. L. Hartvigsen, T. J. Morton, Z. D. Sellers, and J. S. Yoo, 2020, "SPHERE Assembly and Operation Demonstration," INL/EXT-20-60782, Idaho National Laboratory, Idaho Falls, ID, USA. Available: https://gain.inl.gov/MicroreactorProgramTechnicalReports/Document-INL-EXT-20-60782.pdf (accessed 30 June 2022).

[21] Pure World Energy, 2022, "C30 Capstone Microturbine," https://www.pureworldenergy.com/technology/capstone-products/c30-capstone-microturbine/#:~:text=C30%20Capstone%20Microturbine&text=The%20C30%20is%20part%20of,for%20today's%20distributed%20generation%20needs. (accessed 30 June 2022).

[22] Wright, S. A., R. J. Lipinski, M. E. Vernon, and T. Sanchez, 2006, "Closed Brayton Cycle Power Conversion Systems for Nuclear Reactors: Modeling, Operations, and Validation," SAND2006-2518, Sandia National Laboratories, Albuquerque, NM, USA. Available: https://www.osti.gov/servlets/purl/1177051 (accessed 30 June 2022).

[23] Guillen, D. P., and D. S. Wendt, 2020, "Integration of a Microturbine Power Conversion Unit in MAGNET," INL/EXT-20057712, Idaho National Laboratory, Idaho Falls, ID, USA. Available: https://inldigitallibrary.inl.gov/sites/sti/sti/Sort_26619.pdf (accessed 30 June 2022).

[24] Guillen, D. P., and D. S. Wendt, 2021, "Technical feasibility of integrating a modified power conversion unit into a non-nuclear microreactor testbed," *Int. J. Energy Res.*, vol. 45, no. 8, pp. 12325–12343. https://doi.org/10.1002/er.6517.

[25] P. Szymanski and D. Mikielewicz, "Additive Manufacturing as a Solution to Challenges Associated with Heat Pipe Production," *Materials,* vol. 15, no. 4, p. 1609, 2022.

[26] D. P. Guillen, C. G. Turner, A. R. Wagner, and P. J. Moo, "Additive Manufacturing of Heat Pipes for Microreactor Applications," Idaho National Lab.(INL), Idaho Falls, ID (United States), 2020.

[27] D. Lehmhus *et al.*, "Customized smartness: a survey on links between additive manufacturing and sensor integration," *Procedia Technology,* vol. 26, pp. 284-301, 2016.

[28] I. Tomaz *et al.*, "The development of a smart additively manufactured part with an embedded surface acoustic wave sensor," *Additive Manufacturing Letters,* vol. 1, p. 100004, 2021.

[29] Play with Junk YouTube Channel, 2018, "Heat pipes and other thermal stuff (PWJ81)," https://www.youtube.com/watch?v=0oDDHhCPkGA (accessed 30 June 2022).

[30] Lomperski, S., C. Gerardi, and D. Lisowski, 2016, "Fiber optic distributed sensors for high-resolution temperature field mapping," *J. Vis. Exp.*, no. 117, p. e54076. https://doi.org/10.3791/54076.

[31] Bersan, S., L. Schenato, A. Rajendran, L. Palmieri, S. Cola, A. Pasuto, and P. Simonini, 2017, "Application of a high resolution distributed temperature sensor in a physical model reproducing subsurface water flow," *Measurement,* vol. 98, pp. 321–324. https://doi.org/10.1016/j.measurement.2015.09.018.

[32] Lisowski, D. D., C. D. Gerardi, and S. W. Lomperski, 2015, "Thermal cycling testing of distributed fiber optic temperature sensors for high-temperature applications," in *Proc. 16th Int. Top. Meeting Nucl. React. Thermal Hydraul.(NURETH)*, pp. 1–12.

[33] Gerardi, C., N. Bremer, D. Lisowski, and S. Lomperski, "Distributed temperature sensor testing in liquid sodium," *Nucl. Eng. Des.,* vol. 312, pp. 59–65. https://doi.org/10.1016/j.nucengdes.2016.06.017.

[34] Salah, M., A. Bereak, M. Gabry, T. Shaheen, and M. Kewan, 2015, "A Holistic Stimulation Approach to Unlock Potential of Horizontal Open Hole Completion in Tight Carbonate: Optimization of Acidizing Treatment and Successful Diversion in Real-Time Using Distributed Temperature Sensing," in *Abu Dhabi International Petroleum Exhibition and Conference*, 9–12 November 2015, Abu Dhabi, UAE. OnePetro. https://doi.org/10.2118/177800-MS.

[35] Petrie, C. M., N. Sridharan, A. Hehr, M. Norfolk, and J. Sheridan, 2019, "High-temperature strain monitoring of stainless steel using fiber optics embedded in ultrasonically consolidated nickel layers*," *Smart Mater. Struct.,* vol. 28, no. 8, p. 085041. Available: https://iopscience.iop.org/article/10.1088/1361-665X/ab2a27/pdf (accessed 30 June 2022).

[36] Hyer, H. C., D. C. Sweeney, and C. M. Petrie, 2022, "Functional fiber-optic sensors embedded in stainless steel components using ultrasonic additive manufacturing for distributed temperature and strain measurements," *Addit. Manuf.*, vol. 52, p. 102681. https://doi.org/10.1016/j.addma.2022.102681.

[37] Hehr, A., and M. Norfolk, 2019, "A comprehensive review of ultrasonic additive manufacturing," *Rapid Prototyp. J.*, pre-print. https://doi.org/10.1108/RPJ-03-2019-0056.

[38] McCormick, N., and J. Lord, 2010, "Digital image correlation," *Materials Today,* vol. 13, no. 12, pp. 52–54. https://doi.org/10.1016/S1369-7021(10)70235-2.

[39] Thai, T. Q., R. S. Hansen, A. J. Smith, J. Lambros, and R. B. Berke, 2019, "Importance of exposure time on DIC measurement uncertainty at extreme temperatures," *Exp. Tech.*, vol. 43, no. 3, pp. 261–271. https://doi.org/10.1007/s40799-019-00313-3.

[40] Sabharwall, P., J. L. Hartvigsen, T. J. Morton, J. Yoo, S. Qin, M. Song, D. P. Guillen, T. Unruh, J. E. Hansel, J. Jackson, J. Gehin, H. Trellue, D. Mascarenas, R. S. Reid, and C. M. Petrie, 2022, "Nonnuclear experimental capabilities to support design, development, and demonstration of microreactors," *Nucl. Technol.*, pre-print. https://doi.org/10.1080/00295450.2022.2043087.

[41] Yilgor I., E. Lan, and S. Shi, 2022 "Design and Thermal-Hydraulic Performance Analysis of a Low-Temperature Heat Pipe Test Facility," *Nucl. Sci. Eng.,* pre-print. https://doi.org/10.1080/00295639.2022.2087835.

[42] Yilgor, I., and S. Shi, 2022, "Scaling laws for two-phase flow and heat transfer in high-temperature heat pipes," *Int. J. Heat Mass Transf.*, vol. 189, p. 122688. https://doi.org/10.1016/j.ijheatmasstransfer.2022.122688.

[43] Shi, S., Y. Liu, I. Yilgor, and P. Sabharwall, 2022, "A two-phase three-field modeling framework for heat pipe application in nuclear reactors," *Ann. Nucl. Energy*, vol. 165, p. 108770.

[44] Shi, S., "Investigation of transients important for heat pipes in microreactors," Thermal-Hydaulics Laboratory Rensselaer Polytechnic Institute. Available: https://www.thl-rpi.com/research (accessed 30 June 2022).

[45] Ahn, T., P.-H. Huang, J. Diaz, A. Manera, and V. Petrov, 2022, "Experimental study on start-up characteristics of a sodium-filled heat pipe, using in-house high-resolution and high-speed radiation-based imaging system," in *19th International Topical Meeting on Nuclear Reactor Thermal Hydraulics (NURETH-19)*, Virtual Meeting, 6–11 March 2022.

[46] Harvard Medical School, 2019, "Radionuclide scanning," Available: https://www.health.harvard.edu/diseases-and-conditions/radionuclide-scanning-a-to-z#:~:text=A%20radionuclide%20scan%20is%20an,into%20a%20vein%20or%20swallowed. (accessed 30 June 2022).

[47] Moszyński, M., M. Kapusta, A. Nassalski, T. Szczęśniak, D. Wolski, L. Eriksson, and C. L. Melcher, 2006, "New prospects for time-of-flight PET with LSO scintillators," *IEEE Trans. Nucl. Sci.,* vol. 53, no. 5, pp. 2484–2488. https://doi.org/10.1109/NSSMIC.2005.1596927.

[48] M. C. Button, "Devolopment of TDLAS Diagnostics for in situ Harsh Environment Water Vapor Temperature, Concentration, and Pressure Measurements," Ph. D. Thesis, 2019.